ACS EARTH AND SPACE CHEMISTRY

Article

Cite This: ACS Earth Space Chem. 2018, 2, 653−672

# Ambient Measurements of Highly Oxidized Gas-Phase Molecules during the Southern Oxidant and Aerosol Study (SOAS) 2013

Paola Massoli,*[,†] Harald Stark,[†,‡,§] Manjula R. Canagaratna,[†] Jordan E. Krechmer,[†,‡,§] Lu Xu,[⊥,▲] Nga L. Ng,[∥,⊥] Roy L. Mauldin, III,[#] Chao Yan,[▽] Joel Kimmel,[†,○] Pawel K. Misztal,[◆,¶,∞] Jose L. Jimenez,[‡,§] John T. Jayne,[†] and Douglas R. Worsnop[†]

[†]Center for Aerosol and Cloud Chemistry, Aerodyne Research Inc., Billerica, Massachusetts 01821, United States
[‡]Cooperative Institute for Research in Environmental Sciences, University of Colorado, Boulder, Colorado 80309, United States
[§]Department of Chemistry, University of Colorado, Boulder, Colorado 80309, United States
[∥]School of Earth and Atmospheric Sciences, Georgia Institute of Technology, Atlanta, Georgia 30332, United States
[⊥]School of Chemical and Biomolecular Engineering, Georgia Institute of Technology, Atlanta, Georgia 30332, United States
[#]Department of Atmospheric and Oceanic Sciences, University of Colorado, Boulder, Colorado 80309, United States
[▽]Department of Physics, University of Helsinki, FI-00560 Helsinki, Finland
[○]Tofwerk AG, CH-3600 Thun, Switzerland
[◆]Department of Environmental Science, Policy and Management, University of California, Berkeley, California 94720, United States
[¶]Department of Civil and Environmental Engineering, University of California, Berkeley, California 94720, United States

Supporting Information

**ABSTRACT:** We present measurements of highly oxidized multifunctional molecules (HOMs) detected in the gas phase using a high-resolution time-of-flight chemical ionization mass spectrometer with nitrate reagent ion ($NO_3^-$ CIMS). The measurements took place during the 2013 Southern Oxidant and Aerosol Study (SOAS 2013) at a forest site in Alabama, where emissions were dominated by biogenic volatile organic compounds (BVOCs). Primary BVOC emissions were represented by isoprene mixed with various terpenes, making it a unique sampling location compared to previous $NO_3^-$ CIMS deployments in monoterpene-dominated environments. During SOAS 2013, the $NO_3^-$ CIMS detected HOMs with oxygen-to-carbon (O:C) ratios between 0.5 and 1.4 originating from both isoprene ($C_5$) and monoterpenes ($C_{10}$) as well as hundreds of additional HOMs with carbon numbers between $C_3$ and $C_{20}$. We used positive matrix factorization (PMF) to deconvolve the complex data set and extract information about classes of HOMs with similar temporal trends. This analysis revealed three isoprene-dominated and three monoterpene-dominated PMF factors. We observed significant amounts of isoprene- and monoterpene-derived organic nitrates (ONs) in most factors. The abundant presence of ONs was consistent with previous studies that have highlighted the importance of $NO_x$-driven chemistry at the site. One of the isoprene-dominated factors had a strong correlation with $SO_2$ plumes likely advected from nearby coal-fired power plants and was dominated by an isoprene-derived ON ($C_5H_{10}N_2O_8$). These results indicate that anthropogenic emissions played a significant role in the formation of low-volatility compounds from BVOC emissions in the region.

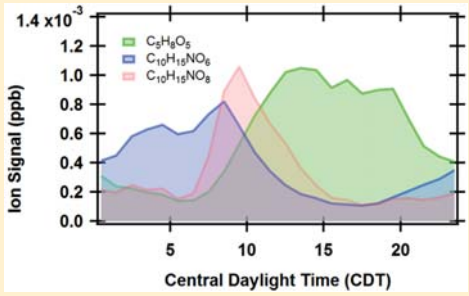


**KEYWORDS:** *high-resolution mass spectrometry, isoprene chemistry, monoterpene chemistry, biogenic−anthropogenic interactions, ambient measurements, positive matrix factorization*

## 1. INTRODUCTION

Recent advances in state-of-the-art chemical ionization (CI) techniques coupled with high-resolution time-of-flight (HRToF) mass spectrometry[1,2] have allowed the detection and quantification at the molecular-formula level of gas-phase organic species with varying degrees of oxygenation, including highly oxidized multifunctional molecules (HOMs).[3−5] HOMs are thought to be key players in new particle formation (NPF) and growth.[6−9] Because of their ability to condense onto aerosol surfaces, HOMs are also considered one of the key missing links in the processes leading to the formation of secondary organic aerosol (SOA).[5,10] The role of HOMs in particle growth is especially critical for SOA formed from biogenic volatile organic compounds (BVOCs), which represent the most abundant VOCs emitted worldwide.[11] For

Received: March 15, 2018
Revised: May 6, 2018
Accepted: May 8, 2018
Published: May 8, 2018






DOI: 10.1021/acsearthspacechem.8b00028
ACS Earth Space Chem. 2018, 2, 653−672

instance, global biogenic emissions of isoprene (600 Tg year$^{-1}$) are considered large enough to result in substantial production of atmospheric particulate matter.[12]

The formation of HOMs from ozonolysis of monoterpene precursors (e.g., $\alpha$-pinene, $\beta$-pinene, limonene) and their proxies (cyclohexene) has been extensively studied in the laboratory[5,8,13−15] using an HRToF CI mass spectrometer with nitrate reagent ion ($NO_3^-$ CIMS.)[16] The $NO_3^-$ CIMS, originally developed to measure sulfuric acid,[17] has proven to be particularly well suited to selective measurement of low-volatility gas-phase molecules with oxygen-to-carbon (O:C) ratios larger than 0.6.[5] Ambient measurements of monoterpene HOMs have been extensively carried out at the SMEAR II boreal forest site in Hyytiälä, Finland, with an atmospheric pressure interface time-of-flight (APi-ToF) mass spectrometer[18] to detect ambient ions both without additional CI[3,4] and with $NO_3^-$ CIMS.[5,19] However, the characterization of isoprene oxidation products via $NO_3^-$ CIMS has until this point been restricted to laboratory studies using flow reactors and environmental chambers.[8,15,20] The Southern Oxidant and Aerosol Study (SOAS) campaign at the Southeastern Aerosol Research and Characterization (SEARCH) ground site at Centreville, Alabama (CTR) from June 1 to July 15, 2013, represented the first field deployment of the $NO_3^-$ CIMS in an isoprene-dominated environment mixed with both terpenes and anthropogenic emissions.[21] Even though the region has seen a significant decrease in sulfur dioxide ($SO_2$) and nitrogen oxides ($NO_x$) over the last two decades,[22] $NO_x$ and particulate sulfate mediated the formation of isoprene-derived SOA during SOAS 2013.[23,24] The $NO_3$ radical (whose concentration was estimated to peak at 1.4 ppt[25]) was also important in the nighttime oxidation of monoterpene[23,26] through the production of organic nitrates (ONs) via termination reactions of organic peroxy radicals ($RO_2$) with $HO_2$.[27,28] Monoterpene-derived ONs comprised 30 to 45% of the gas-phase total reactive nitrogen ($NO_y$) budget at the CTR site.[25] Nitrogen-containing products of isoprene such as isoprene nitrate (ISOPN) and isoprene hydroxynitrates (INs) were also measured using trifluoromethoxy radical ($CF_3O^-$) CIMS[29] and iodide ($I^-$) reagent ion CIMS.[30] Finally, highly functionalized ONs were observed in both the gas and particle phases[31] using an $I^-$ CIMS equipped with a filter inlet for gas and aerosol particles (FIGAERO).[32,33] Particulate ONs contributed 5−10% to total oxygen at the CTR site.[26,31]

Here we report results from the $NO_3^-$ CIMS measurements conducted during SOAS 2013 at the CTR site. Our work provides a comprehensive summary of the gas-phase signals detected and identified via high-resolution (HR) mass spectrometry (1060 gas-phase elemental formulas in total). In order to deconvolve the complexity of the data set, we used positive matrix factorization (PMF) analysis,[34] which has been widely and successfully applied to aerosol mass spectrometer (AMS) data sets[35] and more recently to $NO_3^-$ CIMS unit-mass-resolution (UMR) data.[19] Our PMF analysis was performed on the HR $NO_3^-$ CIMS data. We found that the SOAS 2013 HR $NO_3^-$ CIMS data set can be satisfactorily described by six source factors associated with isoprene- and terpene-derived oxidation products with varying levels of anthropogenic influence. We describe the diurnal profiles and mass spectral features of these factors and interpret them using previous knowledge on the general formation pathways of HOMs from isoprene and monoterpenes, including a direct comparison to previous source characterization of HOMs in a boreal forest environment. Finally, we examine the correlations of our $NO_3^-$ CIMS PMF factors with aerosol factors extracted from PMF analysis performed on a colocated HR-AMS.

## 2. EXPERIMENTAL SECTION

The $NO_3^-$ CIMS (Aerodyne Research Inc. and Tofwerk AG) used in this study combines APi-ToF[18] and a CI inlet that was initially designed to measure $H_2SO_4$.[17] The inlet design is based on a laminar flow reactor where a sample flow is surrounded by a flow of filtered ambient air or zero air. $NO_3^-$ and its higher-order clusters ($(NO_3^-)(HNO_3)$ and $(NO_3^-)(HNO_3)_2$) are produced by exposing air-containing gas-phase $HNO_3$ to a commercial X-ray source (Hamamatsu, photoionizer model L9490). The inlet operates at ambient pressure to minimize wall losses and maximize sensitivity, which is ∼1 ppq following a 15 min average.[16,17] This design makes this source effectively a wall-less reactor, optimal for the detection of low-volatility compounds via clustering or deprotonation without fragmentation.[4] The quantification of product ions is obtained by means of a calibration factor ($C$) that is experimentally derived or computed for $H_2SO_4$ and other organic molecules.[5] In this study, we used the experimentally obtained $C$ value for $H_2SO_4$ ($1.89 \times 10^{10}$ molecules cm$^{-3}$), which was reported for the same inlet configuration and flow through the inlet (a 60 cm long, $^3/_4$ in. diameter sample tube pulling 10 L min$^{-1}$, yielding an inlet transmission efficiency ($f_{inlet}$) of ∼0.7).[5,16] The $H_2SO_4$-based $C$ value provides a lower limit to the reported concentrations of HOMs, which have reaction rates with $NO_3^-$ that are equal to or lower than the one of $H_2SO_4$. Calibrations performed for this instrument after SOAS 2013 with malonic acid, an organic molecule that reacts with $NO_3^-$ at a rate close to the collision limit, yielded a $C$ value of $7.9 \times 10^{10}$ molecules cm$^{-3}$ for a sampling line with $f_{inlet} = 0.07$.[20] For the SOAS 2013 sampling inlet, this corresponds to $C = 0.8 \times 10^{10}$ molecules cm$^{-3}$. Even though the $C$ value for malonic acid is within the theoretical bounds of the expected $C$ values, $(0.4–9.5) \times 10^{10}$ molecules cm$^{-3}$,[5] we chose the $C$ value obtained for $H_2SO_4$ as a lower limit to avoid overestimating HOM concentrations. The data set was also corrected for relative ion transmission versus mass-to-charge ratio ($m/z$) in the instrument using a depletion method.[36,37] A transmission correction curve was obtained experimentally and applied to all of the data reported in this paper. A detailed description of the transmission correction and its results is provided in section S1 in the Supporting Information.

During SOAS 2013, the $NO_3^-$ CIMS operated in "V-mode" and acquired complete mass spectra at rates of 20 kHz with a mass resolving power of ∼3500 M/dM and a mass accuracy of ∼5 ppm. The instrument was manually zeroed every day for 15 min by placing a HEPA filter at the inlet entrance while sampling ambient air, allowing background measurements. The background signals were found to be negligible. The data analysis was performed using the custom software package "Tofware" (version 2.5.10),[38] which enables $m/z$ calibration, baseline corrections, and assignment of a molecular formula to each ion identified by HR analysis. An example of peak identification is shown in the inset of the $NO_3^-$ CIMS campaign-average mass spectrum in Figure S2. PMF analyses were performed using the PMF2.exe algorithm in robust mode.[34] The PMF inputs (mass spectral and error matrices of ∼1000 ions between $m/z$ 160 and 620) were prepared in Tofware, and the solutions were evaluated with the Igor Pro-based PMF Evaluation Tool (version 2.07).[35,39] Additional


DOI: 10.1021/acsearthspacechem.8b00028
ACS Earth Space Chem. 2018, 2, 653−672

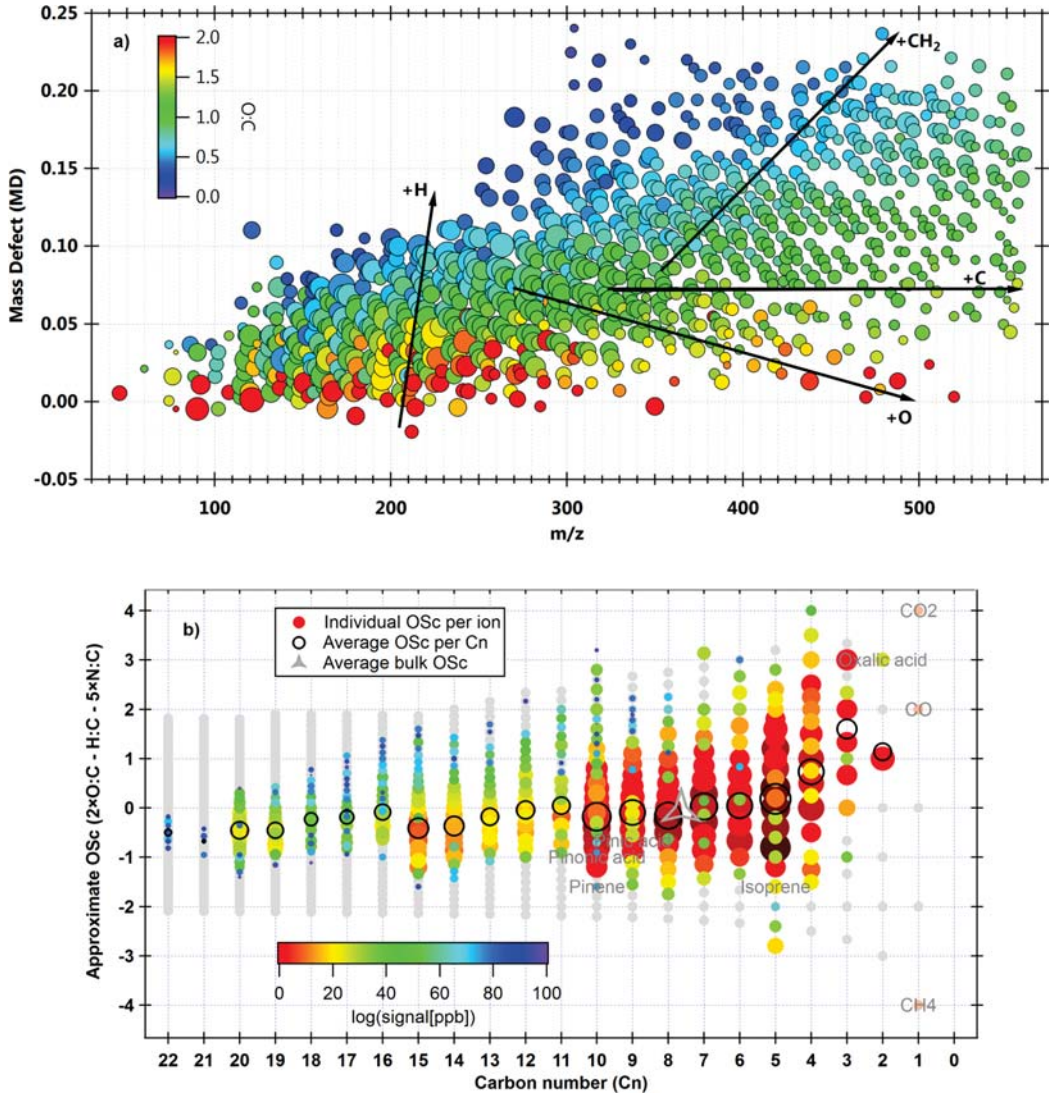


**Figure 1.** (a) Mass defect (MD) plot of the ions identified by HR analysis in the $NO_3^-$ CIMS data set. Data are color-coded by O:C and sized by the percentage of peak area. Trajectories indicating the addition of H, O, or C atoms are shown. The campaign average O:C was 0.91. (b) Average approximate oxidation state ($OS_c$) of the identified ions plotted against the corresponding carbon number ($C_n$). To allow comparison to both gas-phase and aerosol loading, data points are color-coded by log(signal) and scaled by log(signal × $m/z$). The campaign average $OS_c$ was −0.043. Known molecules (pinene, pinonic acid, isoprene, $CH_4$, $CO_2$) are shown in the $OS_c$ vs $C_n$ space as references.

information on the PMF diagnostics and error analysis is provided in section S2 in the Supporting Information.

The data reported here were collected between June 22 and July 13, 2013. We collected data at 1 Hz and averaged to 60 s for postprocessing. It is worth noting that the SOAS 2013 campaign represented the first instance of $NO_3^-$ CIMS deployment under conditions of elevated temperatures and high humidity, with relative humidity (RH) typically around 80%.[22] Previous ambient measurements have mostly occurred at much lower absolute humidities.[5,19] When the sample gas-phase $H_2O$ concentration is high, it is possible for some of the $NO_3^-$ reagent ions to form clusters with $H_2O$ and for these clusters to behave as reagent ions. Such changes in reagent ion identity and distribution can affect the quantification and sensitivities of the $NO_3^-$ CIMS detection scheme. During SOAS 2013, we observed significant amounts of the $NO_3^-(H_2O)$ cluster signal at $m/z$ 80 as well as smaller amounts of higher-order water clusters. We believe that water clusters could be formed during the ionization process or in the weak supersonic expansion that occurs between the source and the first small segmented quadrupole (SSQ) region. Results from several tests performed in the laboratory after the campaign are shown in Figure S3, where the percentage changes in the ratios of the water cluster $NO_3^-(H_2O)$ ($m/z$ 80) to the nitrate reagent ions $NO_3^-$ ($m/z$ 62) and $NO_3^-(HNO_3)$ ($m/z$ 125) are shown as functions of the pressure in the SSQ. We observe a dependence of these ratios on ambient humidity (40% vs 60%). This dependence indicates that the clustering between $NO_3^-$ and $H_2O$ occurs as the sample enters the SSQ region and not during ionization when the sample mixes with the $NO_3^-$ reagent ion. The SSQ pressure during SOAS 2013 was very stable, around 1.96 mbar. Thus, we expect that the high-RH conditions had a negligible effect on the $NO_3^-$ CIMS detection scheme and did not affect quantification of HOMs. However, we did observe large diurnal variations in the reagent ions throughout the campaign that were likely due to the


DOI: 10.1021/acsearthspacechem.8b00028
ACS Earth Space Chem. 2018, 2, 653−672

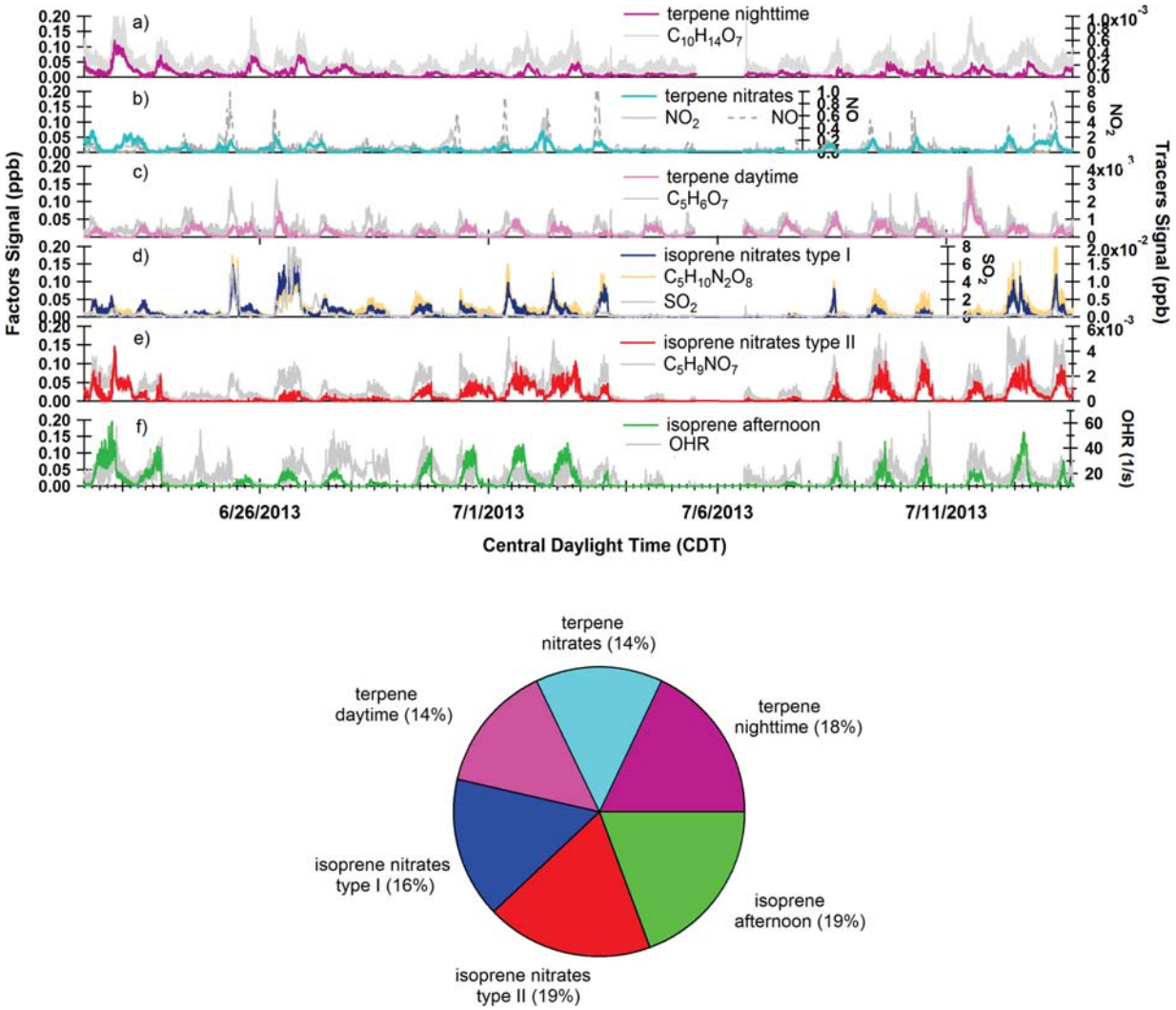


**Figure 2.** Time series of PMF factors (left axes) and tracers from $NO_3^-$ CIMS or other gas-phase instruments (right axes), reported as functions of the local time at the SOAS site. The clustering reagent ion $NO_3^-$ has been omitted from the $NO_3^-$ CIMS formulas to make the labels more readable. Panels (a) through (f) are for the factors terpene nighttime, terpene nitrates, terpene daytime, isoprene nitrates type I, isoprene nitrates type II, and isoprene afternoon. All of the data are reported in parts per billion except for the OH reactivity (OHR), which is reported in $s^{-1}$. The mass percentage fraction of each PMF factor is reported in the pie chart. The fractions ranged from 14% to 19%.

combined effects of diurnal changes in temperature and RH. In order to reduce these effects on the reported HOM concentrations, all of the data have been normalized to the sum of the nitrate clusters ($NO_3^-$, $NO_3^-(HNO_3)$, and $NO_3^-(HNO_3)_2$) plus the water cluster $NO_3^-(H_2O)$. All of the ions reported in this paper were clustered with $NO_3^-$ (only a small number of unclustered ions at $m/z$ below 150 were observed in the data set). For simplicity, all of the molecular formulas are reported without the cluster ion $NO_3^-$.

## 3. RESULTS

**3.1. Bulk Properties of the SOAS Data Set.** Here we present the overall properties of the gas-phase molecules collected during the SOAS 2013 deployment. Commonly used visualizations of complex mass spectrometry data sets are the mass defect (MD) plot[40] and the oxidation state ($OS_c$) plot of ion signals as a function of the carbon number, $C_n$.[41] The MD plot displays the accurate mass of a compound on the $x$ axis and the deviation from the nominal mass (i.e., the mass defect) on the $y$ axis. The addition of oxygen atoms makes the mass defect more negative, while addition of hydrogen atoms makes the mass defect more positive. Thus, the MD plot can be used to assign formulas on trajectories that represent specific modifications or chemical transformations such as oxidation. The MD plot of the HR $NO_3^-$ CIMS data set (Figure 1a) shows bands of ion signals throughout the $m/z$ space, in both the isoprene-dominated region ($m/z$ 180−260) and the monoterpene region ($m/z$ 300−600). Ion bands with different slopes based on H, O, $CH_2$ and +C/−O modifications can be visually identified, as indicated by the arrows in the plot. Similarly to previous reports for other laboratory and ambient CIMS data sets,[33,42] the MD plot illustrates the extremely large number of clusters observed in a typical CIMS data set. Figure 1b shows the average approximate $OS_c$ of each gas-phase ion identified in the HR mass spectrum plotted against the corresponding $C_n$. Functionalization (addition of functional groups, leading to lower-volatility products), fragmentation (loss of carbon, leading to higher-volatility products), and


DOI: 10.1021/acsearthspacechem.8b00028
ACS Earth Space Chem. 2018, 2, 653−672

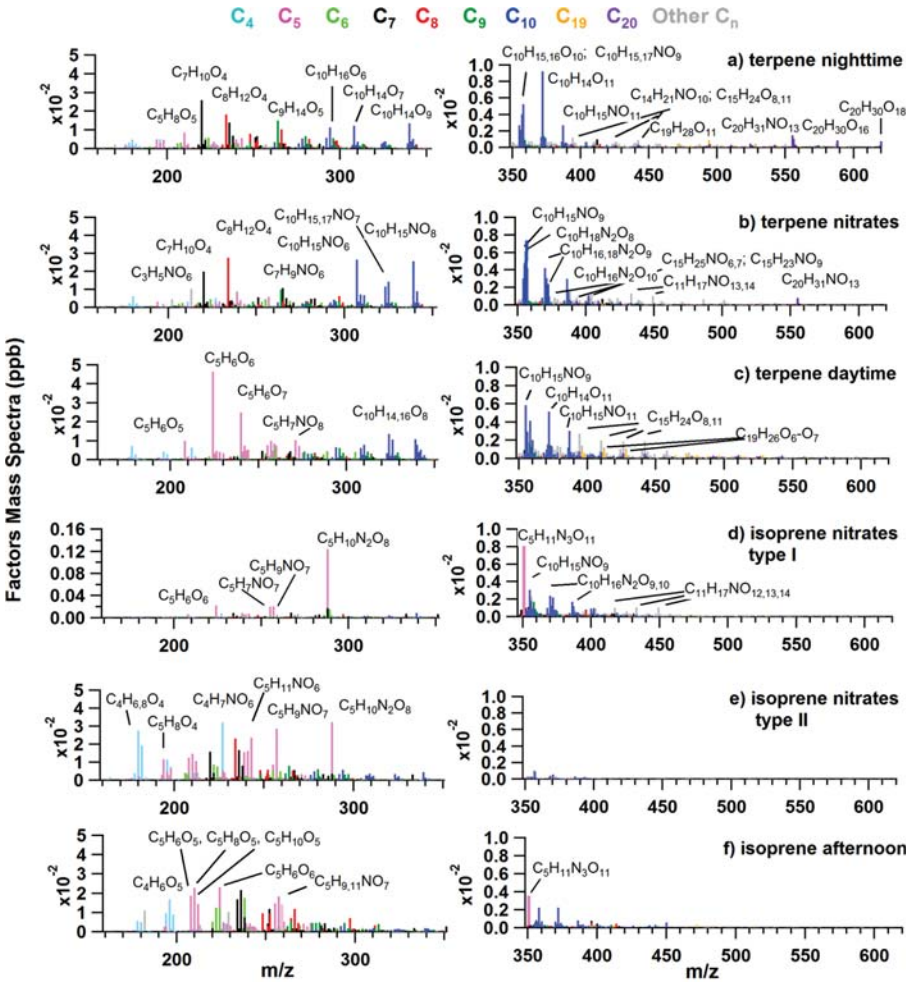


**Figure 3.** Mass spectra of the six PMF factors color-coded by $C_n$ family as indicated at the top of the figure. The left panels show the mass spectra up to $m/z$ 350, and the right panels show the mass spectra from $m/z$ 350 to 620 on a different $y$-axis scale. The clustering reagent ion $NO_3^-$ has been omitted from the formulas to make the labels more readable.

oligomerization are the main chemical processes governing the evolution pathways of molecules in the atmosphere and can be used to interpret the relationship between $OS_c$ and $C_n$.[41,43] The original $OS_c$ formula ($OS_c = 2 \times O{:}C - H{:}C$) was modified to include nitrogen (N). It was assumed that all nitrogen occurred in nitrate ($-ONO_2$) groups as $C-O-NO_2$ since those functional groups would more likely be detected with the $NO_3^-$ CIMS. However, it is important to note that polyfunctional nitrogen-containing species with reduced N functionalities (i.e., heterocycles, amines, or nitriles) could still be detected with the $NO_3^-$ CIMS if they contain enough OH/OOH groups. A group $OS_c$ oxidation state of −1 was used for $-ONO_2$, increasing the $OS_c$ by 1 per carbon atom. This results in two modifications of the original formula, one to account for the nitrate groups and one for the reduced number of oxygen atoms for the O:C ratio:

$$OS_c = 2 \times (O - 2 \times N){:}C - H{:}C + N{:}C \quad (1a)$$

which can be rewritten as

$$OS_c = 2 \times O{:}C - H{:}C - 5 \times N{:}C \quad (1b)$$

effectively modifying the original formula by the term "$-5 \times$ N:C" to account for $-NO_2$ functionalities. This formula is valid only if there is enough oxygen to account for the $-ONO_2$ groups, and therefore, is it applicable only if $O \geq 2 \times N$. All formulas included in the peak list fulfill the $O \geq 2 \times N$ condition, further indicating that it is likely that all of the detected nitrogen occurs in $-ONO_2$ groups. The molecular composition of the SOAS 2013 data set included a wide range of species with $OS_c$ ranging from −1 to +3.5. The average $OS_c$ varied between −0.5 (for $C_{20}$ species) and +1.5 (for $C_3$ species). The O:C, H:C, and N:C campaign averages were 0.91, 1.51, and 0.06, respectively. The $OS_c$ campaign average was −0.043, and the average $C_n$ was 7.5.

**3.2. PMF Analysis.** Results of the PMF analysis performed on the HR $NO_3^-$ CIMS SOAS data set are discussed in this section. A six-factor solution was chosen to describe the data set (see Figure S4 for the full diagnostics of the six-factor solution). The PMF factors were identified on the basis of their unique time series and mass spectral features, shown in Figures 2 and 3, respectively. Three monoterpene-related factors and three isoprene-related factors were identified. The pie chart in Figure 2 shows that all of the factors had comparable mixing ratio abundances (14 to 19%), with the isoprene-related factors having a slightly larger total mass fraction (54%). In Figure 3, the PMF mass spectra are color-coded by the $C_n$ families, $C_4$ through $C_{20}$. On the basis of previous work, isoprene gas-phase products are mainly represented by $C_4$ and $C_5$ ions,[20] whereas


DOI: 10.1021/acsearthspacechem.8b00028
ACS Earth Space Chem. 2018, 2, 653−672

monoterpene products are represented by $C_7$, $C_8$, $C_9$, and $C_{10}$ ions (monoterpene monomers) and $C_{18}$, $C_{19}$, and $C_{20}$ ions (monoterpene dimers).[4,5,8,19,44] Table 1 reports fingerprint molecules for each of the six final PMF factors. PMF solutions with up to 10 factors were also checked, and Figure S5 reports the source allocation from two to 10 factors. The 10-factor solution has a lower residual (4%) compared with the six-factor solution (7%). However, solutions with more than six factors did not provide new process-specific information and made the interpretability of the results more difficult because of factor splitting and fewer unique correlations with external tracers.

**Table 1. Suggested Elemental Composition of Fingerprint Molecules Identified at High Resolution for the Six $NO_3^-$ CIMS PMF Factors (The Clustering Reagent Ion $NO_3^-$ Has Been Omitted from the Formulas)**

| factor | fingerprint molecules |
|---|---|
| terpene nighttime | $C_9H_{14}O_5$, $C_{10}H_{16}O_6$, $C_{10}H_{14}O_7$, $C_{10}H_{16}O_6$, $C_{10}H_{14}O_{11}$, $C_{20}H_{30}O_{16}$, $C_{20}H_{30}O_{18}$, $C_{20}H_{31}NO_{13}$ |
| terpene nitrates | $C_{10}H_{15}NO_6$, $C_{10}H_{17}NO_7$, $C_{10}H_{15}NO_8$, $C_{10}H_{18}N_2O_8$, $C_{10}H_{16}N_2O_9$, $C_{11}H_{17}NO_{13,14}$ |
| terpene daytime | $C_5H_6O_5$, $C_5H_6O_6$, $C_5H_6O_7$, $C_{10}H_{14}O_8$, $C_{15}H_{24}O_{8-11}$ |
| isoprene nitrates type I | $C_5H_{10}N_2O_8$, $C_5H_{11}N_3O_{11}$, $C_5H_{7,9}NO_7$ |
| isoprene nitrates type II | $C_4H_7NO_6$, $C_5H_{11}NO_6$, $C_5H_9NO_7$, $C_4H_{6,8}O_4$ |
| isoprene afternoon | $C_4H_6O_5$, $C_5H_{6,8,10}O_5$, $C_{14}H_{18}O_{22}$, $C_{15}H_{18}O_{15}$, $C_{15}H_{20}O_{18}$ |

The diurnal cycles of the total mixing ratios of the six PMF factors are shown in Figure 4a along with diurnal profiles of NO, $NO_2$, and $O_3$ (in ppb) and solar radiation (SR) (in W $m^{-2}$). The $NO_2$ and NO diurnal cycles show a maximum at 05:30 and 07:30 local time (Central Daylight Time, CDT), respectively, whereas $O_3$ has a daytime maximum at 16:00. The six factors were identified as (1) "terpene nighttime" factor, peaking at 20:00; (2) "terpene nitrates" factor, peaking around 08:30; (3) "terpene daytime" factor, peaking at 12:00; (4) "isoprene nitrates type I" factor, peaking at 09:30 and exhibiting a second small enhancement at 17:30; (5) "isoprene nitrates type II" factor, characterized by two clear diurnal peaks at 12:00 and 19:30; and (6) "isoprene afternoon" factor, showing a broad maximum between 13:00 and 18:00. We chose the generic name "terpene" rather than, e.g., $\alpha$-pinene because during SOAS 2013 the monoterpene emissions were a combination of $\alpha$-pinene and $\beta$-pinene with additional quantities of limonene and smaller amounts of camphene and myrcene.[25]

In addition to the different "peak times", each factor diurnal profile has other unique characteristics, with different increasing and decreasing profiles. For instance, the terpene nitrates profile rises and decreases sharply, while the isoprene nitrates type II factor has a less steep rising trend and a broader presence throughout the day. We also notice that the terpene nighttime factor is still present during the day at low concentrations (~0.01 ppb). In contrast, the terpene daytime, isoprene afternoon, and isoprene nitrates type I factors approach zero levels overnight, suggesting that their formation is driven by daytime photochemistry only. Other factors have higher backgrounds either after sunset (~19:30), as in the case of the isoprene nitrates type II factor, or before sunrise (~05:30), as in the case of the terpene nitrates factor. All of these different trends point to the existence of specific chemical processes involved in the formation of the isoprene and terpene oxidation products pooled in each factor. The diurnal profiles of the isoprene afternoon, isoprene nitrates type I, and terpene daytime factors suggest a decay lifetime of about 2 h after the end of the photochemically active period. The time scale for condensation onto the aerosol for nonvolatile species was estimated to be on the order of 30 min at this site.[20] Since all of the factors include a significant fraction of semivolatile species, loss to the aerosol likely explains much of these decays. Dry deposition to surfaces may also contribute to the decays but is expected to be slower.[29] We are also aware that these diurnal cycles were impacted by changes in the planetary boundary layer (PBL), which ranged from ~700 m at night to ~1200 m during the day and was stable at night.[23,25,45] We did not apply a correction for changes in PBL height to this data set.

Figure 4b shows the contribution of each factor to $C_n$ ranging from 0 to 22 (we report the factor intensities as normalized signals for better comparison of the factor profiles). The plot shows that all of the isoprene factors peak at $C_5$, with a tail going up to $C_{10}$, which could be a result of $RO_2$ + $RO_2$ chemistry. All of the terpene factors instead peak at $C_{10}$, but one of them (terpene daytime) has a strong $C_5$ peak as well, which we attribute to $C_5$ products resulting from terpene fragmentation, as discussed later in more detail. The terpene factors also have smaller peaks at $C_{20}$ (terpene dimers) and $C_{15}$, which again could indicate $RO_2$ + $RO_2$ (mixed terpene + isoprene or terpene + $C_5$ terpene fragments) but could also be indicative of sesquiterpenes. Finally, a secondary peak at $C_8$ is observed in both terpene nighttime and terpene nitrates; this is expected, as $C_8$ compounds have been observed in the oxidation of monoterpenes.[8] The slight enhancement of $C_8$ in the isoprene factors as well could indicate mixing of PMF factors or the existence of non-monoterpene $C_8$ compounds. Figure S6 shows additional diagrams of the approximate $OS_c$ as a function of $C_n$ (Figure S6a) and the normalized factor signal as a function of $OS_c$ along with the average $OS_c$ for each factor (Figure S6b). The decrease in $OS_c$ with $C_n$ is similar for all of the factors, while the distribution of the normalized signal as a function of $OS_c$ is slightly different for each factor, with average $OS_c$ varying from −0.14 (terpene nitrates) to +0.36 (isoprene afternoon). The more negative $OS_c$ values reflect lower O:C ratios and/or more $-NO_2$ groups, while the more positive $OS_c$ values indicate higher O:C ratios and/or fewer $-NO_2$ groups. The following sections describe each of the PMF factors in further detail.

**3.3. Terpene-Related Chemistry.** *3.3.1. Terpene Nighttime Factor.* The terpene nighttime factor had its maximum peak at 20:00 CDT (Figure 4). Its mass spectrum (Figure 3a) was mainly characterized by $C_7$, $C_8$, $C_9$, and $C_{10}$ ions, among which the highest are $C_7H_{10}O_4$, possibly a myrcene fragment,[8] and several terpene monomer products in the $C_{10}H_{14}O_{7-11}$ and $C_{10}H_{16}O_{7-11}$ series. Monoterpene $C_{19}$ and $C_{20}$ dimers with formulas $C_{19-20}H_{28,30}O_{11-16}$ were also observed. Previous studies have discussed the formation of $\alpha$-pinene HOM dimers via a $RO_2$ + $RO_2$ channel.[5] The terpene nighttime factor time series (Figure 2a) showed a strong correlation with the time series of $C_{10}H_{14}O_7$ ($m/z$ 308), one of the fingerprint molecules in this factor that has a stronger nighttime maximum. $C_{10}H_{15}O_{10}$ and $C_{10}H_{16}O_{10}$ at $m/z$ 357 and 358 were also enhanced. These ions have all been observed in the monoterpene-dominated boreal forest and in laboratory studies mainly, but not exclusively, under ozonolysis (e.g., nighttime) conditions.[4,5,8] The PMF analysis of the $NO_3^-$ CIMS data



DOI: 10.1021/acsearthspacechem.8b00028
ACS Earth Space Chem. 2018, 2, 653−672

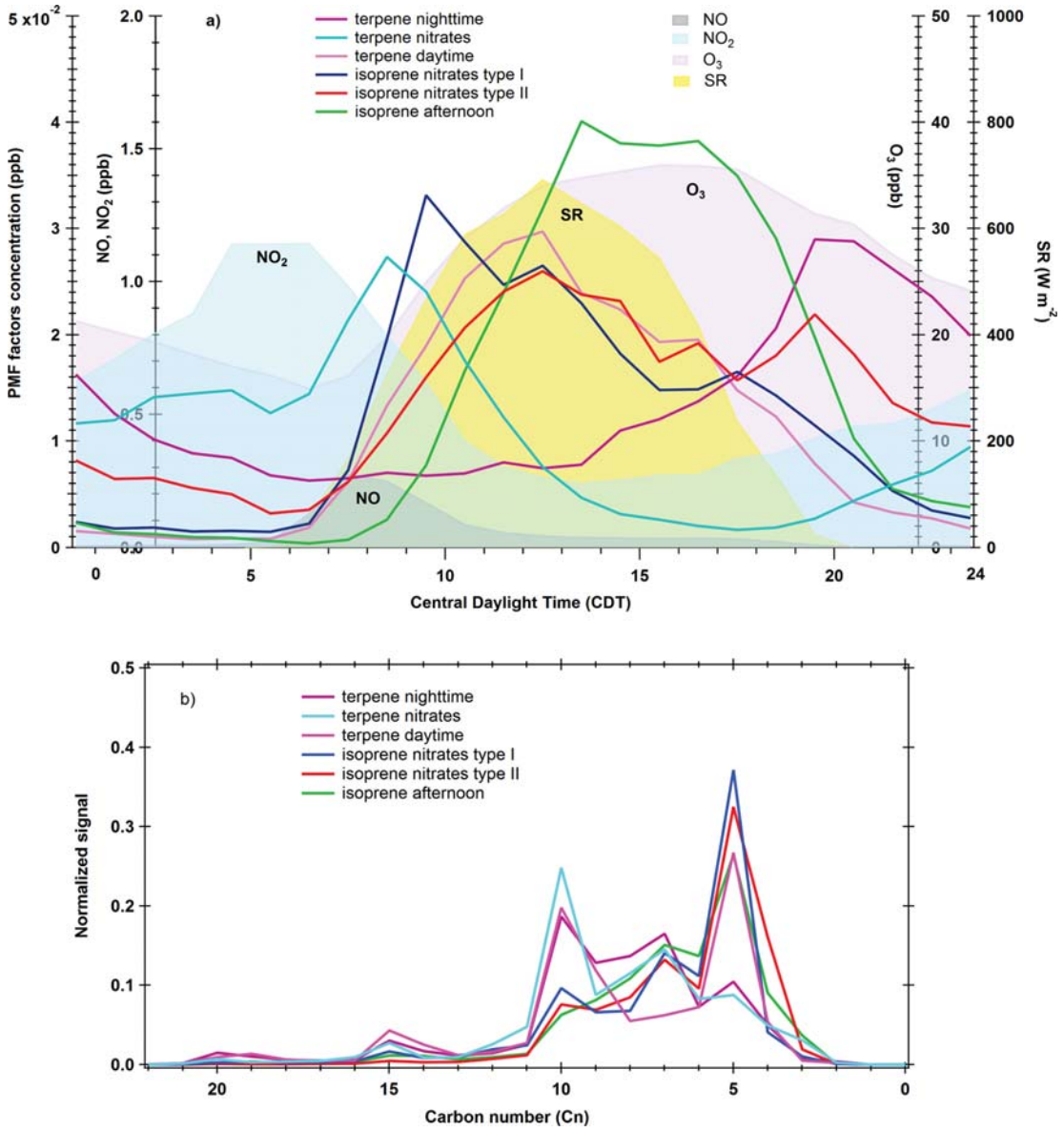


**Figure 4.** (a) Diurnal cycles of the six PMF factors. The diurnal profiles are reported as functions of the local time at the CTR site. The diurnal profiles of NO, $NO_2$, $O_3$, and solar radiation (SR) are also shown. (b) Contribution of each factor (as normalized signal) to $C_n$. Terpene factors have most of the signal at $C_n > 5$, while isoprene factors have most of signal at $C_n \leq 5$.

collected in Hyytiälä, Finland, also reported these same HOMs in a type I nighttime PMF factor that has been explained by oxidation processes driven by $O_3$.[19] As expected, the terpene nighttime factor was best correlated with monoterpene BVOCs measured using a proton transfer reaction time-of-flight mass spectrometer (PTR-ToF-MS)[45] and with other monoterpene species, as shown in the correlation plot with external tracers in Figure 5a.

The mass spectrum of the terpene nighttime factor also shows several nitrogen-containing products such as $C_{10}H_{15}NO_{9,11}$ ($m/z$ 387) and $C_{20}H_{31}NO_{13}$ ($m/z$ 555), likely originating from $NO_3$-radical-initiated oxidation. The mechanism for the formation of gas-phase organic nitrates ($RONO_2$) from the reaction of both $\alpha$- and $\beta$-pinene with $NO_3$ radical has been discussed in previous ambient and laboratory data sets[27,28,46] and has been shown to be important during SOAS 2013.[23,25,26,31] The same ON ions were found in a nighttime type II factor in Hyytiälä.[19] For this data set, however, we were not able to clearly separate two nighttime monoterpene factors (one containing HOM terpene monomers and dimers and the other containing ON terpene dimers), even when going to 10 or 12 factors. We also measured a lower abundance of terpene $C_{20}$ dimers at the CTR site during the nighttime compared with the Hyytiälä data set.[19] The dimer:monomer ($C_{20}$:$C_{10}$) ratio in Hyytiäla is about 20−30% in nighttime conditions,[47] whereas we obtained a nighttime $C_{20}$:$C_{10}$ ratio of ∼5% during SOAS 2013. However, much lower (<10%) $C_{20}$:$C_{10}$ ratios have been observed in Hyytiälä with higher $NO_x$ mixing ratios, typically measured during the daytime.[47] It has been indeed suggested that high NO concentration (>1 ppb) and a low $RO_2$:$HO_2$ ratio can suppress dimer formation.[5] Recent laboratory work[15] reported a $C_{20}$:$C_{10}$ ratio of 0.1 under low-$NO_x$ conditions and a ratio of 0.04 under high-$NO_x$ conditions, supporting the hypothesis of $NO_x$-driven suppression of terpene dimer


DOI: 10.1021/acsearthspacechem.8b00028
ACS Earth Space Chem. 2018, 2, 653−672

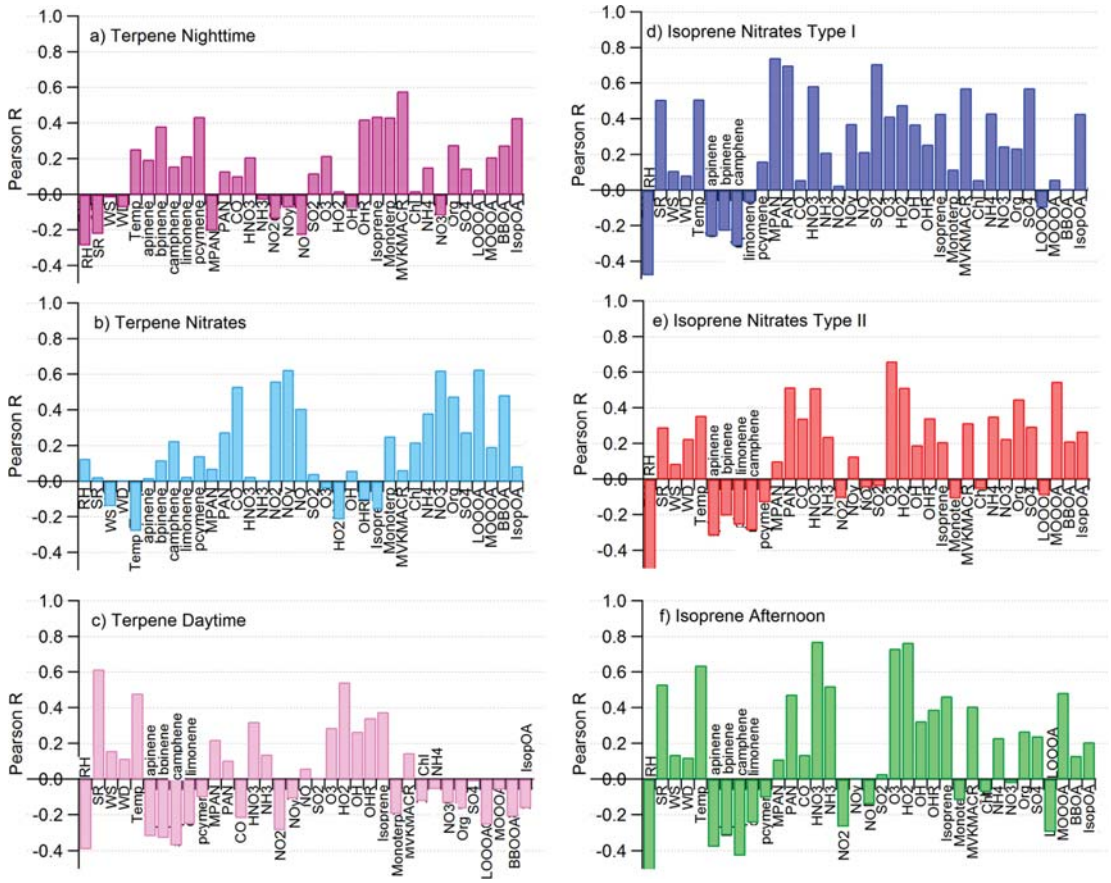


**Figure 5.** Correlations of (a−c) terpene-related and (d−f) isoprene-related PMF factors with external gas-phase and particulate tracers from other instruments deployed at the CTR site. From left to right, the tracers are meteorological data (relative humidity (RH), solar radiation (SR), wind direction (WD), wind speed (WS), and temperature (Temp)), monoterpene species ($\alpha$-pinene, $\beta$-pinene, camphene, limonene, and $p$-cymene), gas-phase species (methyl peroxy acyl nitrate (MPAN), PAN, CO, $HNO_3$, $NH_3$, $NO_2$, $NO_y$, NO, $SO_2$, $O_3$, $HO_2$, OH, and OH reactivity (OHR)), PTR-ToF-MS species (isoprene, monoterpenes, and methyl vinyl ketone/methacrolein (MVK/MACR)), HR-AMS species (particle Chl, $NH_4$, $NO_3$, organics (Org), and $SO_4$), and PMF factors (less oxygenated organic aerosol (LO-OOA), more oxygenated organic aerosol (MO-OOA), burning biomass organic aerosol (BBOA), and isoprene organic aerosol (Isop-OA)).

formation. Compared to Hyytiälä,[19] the NO and $NO_2$ loadings were 2−3 times higher at the CTR site, where the average NO concentration was 0.3 ppb and the $NO_2$ concentration varied between 0.5 and 4 ppb. Measured $HO_2$ concentrations during the SOAS 2013 campaign were between 3 pptv (at night) and 27 pptv (daytime peak),[48] similar to those reported for typical springtime conditions in Hyytiälä. Therefore, the most likely explanation for the low $C_{20}$:$C_{10}$ ratio is that the $NO_x$ amount at the CTR site was high enough to inhibit dimer formation, although we cannot exclude the role of other unknown chemical processes. The higher temperatures might have also decreased the yields of bimolecular radical recombination reactions such as $RO_2$ + $RO_2$, contributing to the lower $C_{20}$:$C_{10}$ ratio observed in SOAS compared with Hyytiälä.

*3.3.2. Terpene Nitrates Factor.* The second terpene-chemistry-related factor in the PMF analysis, which we called terpene nitrates, had a maximum peak at around 08:30 and relatively elevated concentrations during the early morning hours before sunrise (Figure 4). The time series of Figure 2b indicates that the terpene nitrates factor is well-correlated with gas-phase $NO_2$ and NO. The external tracers correlation plot (Figure 5b) further shows that the PMF terpene nitrates factor had the highest correlations (Pearson $R$ = 0.5 to 0.6) with gas-phase $NO_2$, $NO_x$, and CO, suggesting the influence of anthropogenic emissions. We find that this factor contains the bulk of terpene nitrates measured during SOAS 2013. Its mass spectrum (Figure 3b) is characterized by monoterpene ONs belonging to the series $C_9H_{15}NO_{5-7}$, $C_{10}H_{15}NO_{6-10}$, and $C_{10}H_{17}NO_{6-10}$ (of which $C_{10}H_{17}NO_{11}$ is the most intense) as well as dinitrate compounds in the series $C_{10}H_{14}N_2O_{8-11}$ and $C_{10}H_{16}N_2O_{8-11}$ (with the latter series being more intense). The $C_{10}H_{14-18}N_2O_{6-13}$ species are most likely the result of multiple-generation processes involving OH or $NO_3$ oxidation of $\alpha$-pinene (or other monoterpenes) combined with $RO_2$ + NO termination reactions.[15] $C_{10}H_{16}N_2O_7$ was also detected in the particle phase by a colocated FIGAERO $I^-$ CIMS.[31] The terpene nitrates factor also contains elevated levels of $C_7$ and $C_8$ ions, e.g., $C_7H_{10}O_4$ and $C_8H_{12}O_4$. The latter corresponds to the molecular formula of norpinic acid. As noted above, the terpene nitrates factor had a maximum shortly after the NO peak (which occurred around 07:30), but it was also well above zero during the nighttime hours, when the $NO_2$ and $NO_3$ radical concentrations were higher. To look at the contributions of specific ions to this factor, we analyzed the diurnal cycles of the major ONs detected via $NO_3^-$ CIMS. Figure 6a shows monoterpene ON ions that peaked in the morning (around 08:30) but were also elevated at night: the majority of those belong to the series $C_{10}H_{17}NO_{5-10}$, with the exception of



DOI: 10.1021/acsearthspacechem.8b00028
ACS Earth Space Chem. 2018, 2, 653−672

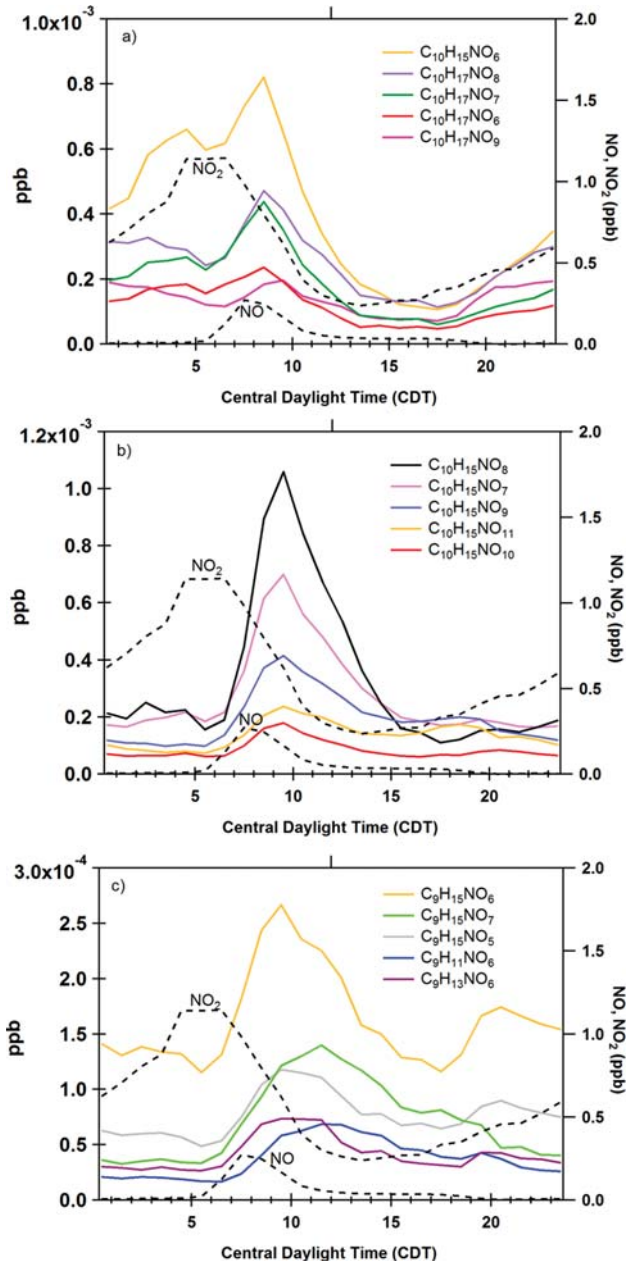


**Figure 6.** Diurnal cycles of the major monoterpene ONs during SOAS 2013 along with NO and $NO_2$: (a) the $C_{10}H_{17}NO_{5-9}$ series and the ion $C_{10}H_{15}NO_6$, which peak around 08:00 but are also elevated at night; (b) the $C_{10}H_{15}NO_{7-11}$ ions, which increase after sunrise, with a maximum at 10:00; and (c) the $C_9$ ONs, which reach their maximum intensity between 09:00 and 12:00. The clustering reagent ion $NO_3^-$ has been omitted from the formulas to make the labels more readable.

$C_{10}H_{15}NO_6$, the most abundant in this group. $C_{10}H_{15}NO_6$ might be formed by $NO_3$ oxidation of pinonaldehyde combined with $NO_2$ termination to form a peroxy acyl nitrate (PAN) species. Recent laboratory studies[28] showed that $C_{10}H_{15}NO_6$ is the most abundant ion observed from $\alpha$-pinene + $NO_3$ and can also be formed in large amounts upon photochemical aging when transitioning from "night" to "day"; however, the overall ON (and SOA) yield from $\alpha$-pinene + $NO_3$ is rather low compared with those from, for example, $\beta$-pinene + $NO_3$ and with most other monoterpenes[28,49,50] that might have contributed to $C_{10}H_{15}NO_6$. The nighttime presence of $C_{10}H_{17}NO_{5-10}$ compounds, which for instance were very low in Hyytiälä,[19] could be explained by $NO_3$-initiated oxidation followed by $HO_2$ termination. The ions in the $C_{10}H_{15}NO_{7-11}$ series instead increased only after sunrise, with a maximum around 09:30, approximately 2 h after the NO peak (Figure 6b); the $C_{10}H_{15}NO_8$ ion[51] was the most abundant in this class. Finally, Figure 6c shows some of the $C_9$ terpene organonitrates, which reached their maximum between 09:00 ($C_9H_{15}NO_6$) and 12:00 ($C_9H_{15}NO_7$); a few of them had a second peak around 20:00. Upon comparison of these ion trends with the diurnal cycle of the terpene nitrates factor in Figure 4, we see that the factor was highly influenced by the $C_{10}H_{15}NO_6$ and $C_{10}H_{17}NO_{5-10}$ ions of Figure 6a that were elevated overnight. The factor peak occurring around 08:30 had additional contributions from other $C_{10}H_{15}$ ONs and from $C_{10}H_{14}$ and $C_{10}H_{16}$ dinitrates (Figure S7). The $C_{10}$ dinitrate ions show a similar trend and decay as the $C_{10}$ monoterpene ONs of Figure 6b, with a sharp increase at 07:00 followed by a peak around 09:30 and a tail lasting through the day. The morning peak at ~09:00 makes our terpene nitrates factor most similar to the Hyytiälä daytime type I factor that was explained by $RO_2$ + NO reactions.[19] However, $C_{10}H_{15}NO_8$ seems to behave differently in the Hyytiälä data set, since it almost constitutes its own factor (daytime type II). The diurnal cycle of the high-resolution signal for $C_{10}H_{15}NO_8$ during SOAS (Figure 6b) clearly excludes the possibility that this discrepancy is a data analysis artifact and points to different formation pathways for $C_{10}H_{15}NO_8$ in these two environments or possibly to the presence of two forms of the same molecule that have different behaviors and formation pathways. It is also worth pointing out that because during SOAS 2013 the terpene emissions were a combination of $\alpha$-pinene, $\beta$-pinene, and limonene, the observed $C_{10}$ ON products likely originated from several types of terpenes.

*3.3.3. Terpene Daytime Factor.* The third and last terpene-chemistry-related factor was a terpene daytime factor characterized by a broad daytime distribution peaking at 12:00 (Figure 4). The external tracers plot (Figure 5c) shows the highest Pearson $R$ values for ambient temperature and solar radiation ($R > 0.5$), while $R$ values between 0.3 and 0.4 were observed for correlations with $HO_2$, $O_3$, OH, and OH reactivity (OHR),[48] all indicators of daytime photochemistry. The mass spectrum of the terpene daytime factor (Figure 3c) was dominated by two $C_5$ compounds ($C_5H_6O_6$ at $m/z$ 224 and $C_5H_6O_7$ at $m/z$ 240) that have been previously reported as $\alpha$-pinene fragmentation products.[4,19] While $C_5$ compounds are most commonly related to isoprene chemistry, we note that neither $C_5H_6O_6$ nor $C_5H_6O_7$ was observed during isoprene or isoprene hydroxyhydroperoxide (ISOPOOH) oxidation experiments in the laboratory.[15,20] In addition, a recent comprehensive review of isoprene chemistry does not list such formulas among the most common isoprene oxidation products.[52] To our knowledge, there is no known or theorized pathway in which the reaction of isoprene with OH produces highly unsaturated $C_5$ compounds (e.g., the level of unsaturation of 3 for $C_5H_6O_6$). Consistent with the interpretation of $C_5H_6O_6$ and $C_5H_6O_7$ as daytime monoterpene decomposition products, they were observed from $\alpha$-pinene OH-driven oxidation under high-$NO_x$ conditions.[15] However, $C_5H_6O_6$ and $C_5H_6O_7$ have also been reported as products of alkene autoxidation under ozonolysis,[14] indicating also the possibility of an anthropogenic source for these ions.



DOI: 10.1021/acsearthspacechem.8b00028
ACS Earth Space Chem. 2018, 2, 653−672

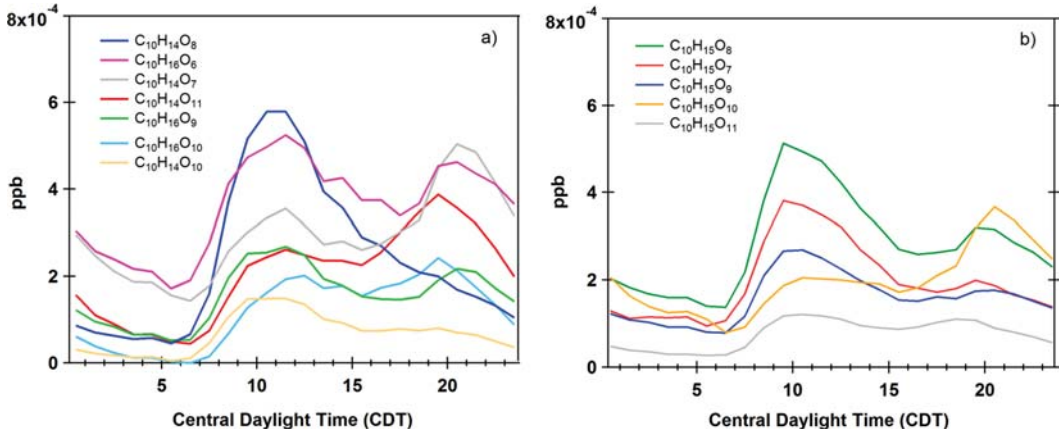


**Figure 7.** Diurnal cycles of the most abundant (a) monoterpene $C_{10}$ closed-shell monomers and (b) $C_{10}$ radicals. With only a few exceptions, many of these compounds have a daytime maximum and a second peak after sunset. The clustering reagent ion $NO_3^-$ has been omitted from the formulas to make the labels more readable.

This PMF factor also contains two monoterpene-related $C_{10}$ ions, $C_{10}H_{14}O_8$ at $m/z$ 324 and $C_{10}H_{16}O_8$ at $m/z$ 326, that seem to be unique to daytime chemistry. The diurnal cycle of $C_{10}H_{14}O_8$ is shown in Figure 7a along with the diurnal cycles of several $C_{10}$ closed-shell monomers that instead had two diurnal maxima, one at 11:00 and one at 20:00, and were allocated by PMF to both the terpene nighttime and daytime factors ($C_{10}H_{14}O_7$ and $C_{10}H_{14}O_{11}$ had instead a much stronger nighttime peak, and they were exclusively allocated to the terpene nighttime factor). Most of the $C_{10}$ open-shell compounds (Figure 7b) also had two peaks in their diurnal cycle and consequentially were allocated to both the terpene nighttime and daytime factors. The only exception was $C_{10}H_{15}O_{10}$, which has a stronger nighttime maximum and was allocated to the terpene nighttime factor (consistently, $C_{10}H_{15}O_{10}$ has been reported as one of the fingerprint molecules of the Hyytiälä nighttime type I factor[19]). The double diurnal peak observed for many of these ions suggests isomeric structures having the same molecular formula, which were reported for several ions by ion mobility spectrometry–mass spectrometry (IMS-MS) during SOAS 2013.[53]

**3.4. Isoprene-Related Chemistry.** *3.4.1. Isoprene Nitrates Type I Factor.* The isoprene nitrates type I factor (Figure 4) had a broad daytime presence, with a peak at ∼09:30 and a second, smaller enhancement at 17:30. Its mass spectral feature (Figure 3d) is almost exclusively dominated by an ion at $m/z$ 288 that we identified with an isoprene dinitrate having the elemental formula $C_5H_{10}N_2O_8$ and by a $C_5$ trinitrate having the elemental formula $C_5H_{11}N_3O_{11}$ at $m/z$ 351. Few other $C_5$ isoprene-related ions below $m/z$ 300 and very little mass above $m/z$ 350 are present in the spectrum. Theoretical studies have shown that $C_5H_{10}N_2O_8$ can be a product of 1,2-isoprene nitrate (ISOPN, $C_5H_9NO_4$), a hydroxynitrate formed via OH-initiated isoprene oxidation at high $NO_x$ concentration.[30] The time series of this PMF factor is shown in Figure 2d along with those of $C_5H_{10}N_2O_8$ and gas-phase $SO_2$ because we noticed that the time profile of gas-phase $SO_2$ was correlated with this factor during two time periods when $SO_2$ was particularly high. During the campaign, $SO_2$ levels were typically around 0.5 ppb, except for a few occasions when $SO_2$ reached 6–8 ppb (June 25–27) and 2 ppb (July 3 and 13). These periods correspond to the maximum enhancement of the isoprene nitrates type I factor and, consequently, of $C_5H_{10}N_2O_8$ and $C_5H_{11}N_3O_{11}$. FLEXPART back-trajectory analysis[54] of the air masses that reached the CRT site during these times are reported in Figure S8. Between June 25 and 27, the air masses were originating from the west-southwest and might have carried $SO_2$ and $NO_x$ emissions from coal-fired power plants located south of the site (Figure S9). On July 3, the air reaching the CTR site was prevalently from the west-northwest, possibly carrying power plant plumes from the Birmingham, AL, area or from locations even further north. Power plant plumes were measured on the night of July 2–3 near the Tennessee, Arkansas, and Missouri border around 20:00 local time, where high levels of $N_2O_5$ and $ClNO_2$ were sampled, but no specific organic molecules from isoprene were reported.[33] However, some studies have reported isoprene chemistry inside $SO_2$- and $NO_x$-rich power plant plumes, leading to the formation of isoprene-derived OA.[55] The tracer plot in Figure 5d shows high Pearson $R$ values ($R \geq 0.6$) between this PMF factor and particle $SO_4$ as measured by the colocated HR-AMS,[23] an expected result given the correlation with gas-phase $SO_2$. We also observe high correlations with PAN and methyl peroxy acyl nitrate (MPAN) (Pearson $R$ of 0.7, and 0.75, respectively), as measured by gas chromatography coupled with electron capture detection.[56] It is worth noting that this is the only factor that has a significant correlation with MPAN, which is a known second-generation product of isoprene photo-oxidation under high-$NO_x$ conditions.[57] The time series of PAN and MPAN indeed showed an enhancement during these time periods, even though they were also elevated at other times. The $C_5H_{10}N_2O_8$ and $C_5H_{11}N_3O_{11}$ ions and other similar multiple ONs ($C_5H_{10}N_2O_{9,10}$ and $C_5H_{11}N_3O_{12}$) were observed in laboratory studies following the reaction of isoprene with OH in the presence of NO.[15] On the basis of the conditions used to reproduce the SOAS 2013 spectra, these laboratory results suggested that the air masses containing high concentrations of isoprene dinitrates were a few days old before reaching the CTR site. This is consistent with the time scales of the FLEXPART model and the fact that dinitrate formation requires two OH additions to the isoprene backbone. However, it is possible that shorter oxidation time scales or different $NO_x$ levels could have generated high di- and trinitrate signals in the laboratory. In general, the photochemical conditions during SOAS 2013 imply higher $NO_x$ levels than the laboratory conditions in order to justify the presence of significant


DOI: 10.1021/acsearthspacechem.8b00028
ACS Earth Space Chem. 2018, 2, 653–672

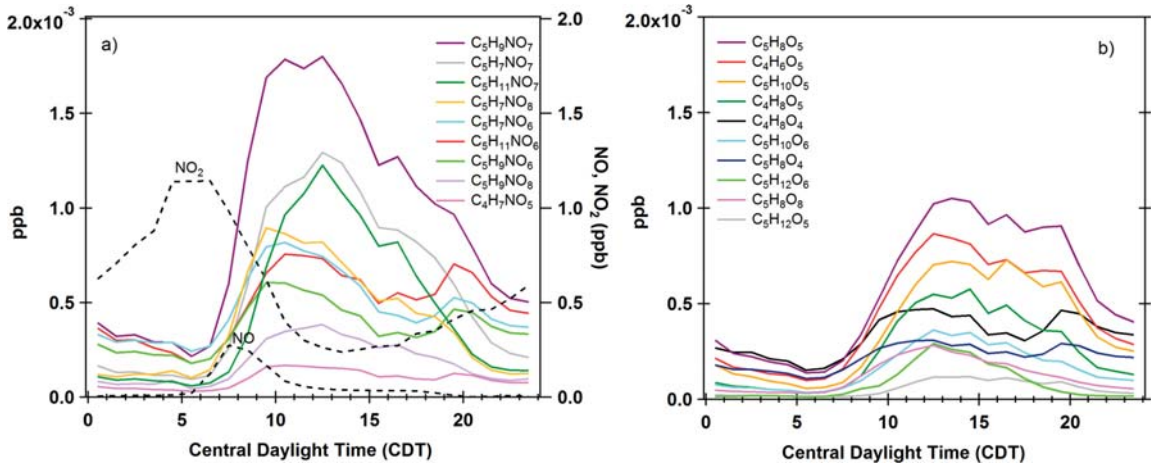


**Figure 8.** Diurnal cycles of the major (a) isoprene ONs and (b) isoprene non-nitrate ions. The HOMs reported in (b) are the same species that were observed to condense on pre-existing aerosol particles during chamber experiments under low $NO_x$ conditions.[20] The clustering reagent ion $NO_3^-$ has been omitted from the formulas to make the labels more readable.

amounts of ONs along with other $RO_2$ + NO termination products.

*3.4.2. Isoprene Nitrates Type II Factor.* The isoprene nitrates type II factor had a unique diurnal cycle (Figure 4), with a broad daytime peak centered between 12:00 and 14:00 and a nighttime presence as demonstrated by a second, less intense peak around 19:30. The mass spectrum (Figure 3e) shows the presence of several $C_4$ and $C_5$ isoprene nitrate products with seven to 11 hydrogen atoms and five to eight oxygen atoms. The most abundant ones were $C_4H_7NO_6$ ($m/z$ 227), $C_5H_7NO_6$ ($m/z$ 239), $C_5H_9NO_6$ ($m/z$ 241), $C_5H_{11}NO_6$ ($m/z$ 243), and $C_5H_9NO_7$ ($m/z$ 257); the time series of the latter matches almost perfectly the time series of the factor (Figure 2e). Other identified isoprene nitrates, present in smaller quantities, were $C_5H_9NO_7$ ($m/z$ 259), $C_5H_7NO_8$ ($m/z$ 271), and $C_5H_9NO_8$ ($m/z$ 273). The isoprene dinitrate $C_5H_{10}N_2O_8$ was also present. The fingerprint ion of this factor, $C_5H_9NO_7$, has been identified with dihydroxy hydroperoxy nitrate (DHHPN), a multigeneration product of ISOPN formed via the $RO_2$ + $HO_2$ reaction.[30] Many of the isoprene nitrates detected by the $NO_3^-$ CIMS during SOAS 2013 have been reported as second- and third-generation OH oxidation products of isoprene under high-$NO_x$ conditions.[15,31] Known first-generation products of isoprene chemistry under high-$NO_x$ conditions, such as ISOPN and methacrolein nitrate/methyl vinyl ketone nitrate (MACRN/MVKN, $C_4H_7NO_5$) were detected only in small quantities, likely because of the low sensitivity of the $NO_3^-$ CIMS toward first-generation products of isoprene chemistry with O:C < 0.6. The diurnal cycles of the relevant isoprene ONs are shown in Figure 8a. The most abundant ions ($C_5H_9NO_{7,8}$ and $C_5H_{7,11}NO_7$) had a single diurnal peak around 12:00, but other less intense isoprene ONs ($C_5H_{7,9,11}NO_6$) had a second peak around 19:30−20:00, consistent with the diurnal profile of the PMF factor (Figure 4). These ions were also observed in laboratory experiments on isoprene oxidation under high-$NO_x$ conditions and varying OH exposures.[15] In addition to isoprene ONs, this factor showed an appreciable presence of $C_5H_8O_4$ ($m/z$ 194), whose elemental composition matches that of DHMOB (dihydroxycarbonyl from $C_5$ hydroxycarbonyl, $HC_5$), another isoprene multigeneration product formed under high-$NO_x$ conditions.[58] The ions $C_4H_6O_4$ ($m/z$ 180) and $C_4H_8O_4$ ($m/z$ 182), which have been observed in previous isoprene chamber experiments under low $NO_x$,[20] were also elevated in the mass spectrum of the isoprene nitrate type II factor. The diurnal cycles of $C_4H_6O_4$ and $C_4H_8O_4$ (Figure 8b) indeed have the same diurnal profile as many other isoprene ONs of Figure 8a (with one peak at 11:00 and one at 20:00), which explains their presence in the isoprene nitrates type II factor. Finally, the correlation with external tracers (Figure 5e) shows positive correlations with the isoprene precursor and MVK/MACR measured by PTR-ToF-MS.[45] $HO_2$, PAN, and $HNO_3$ also correlate positively (Pearson $R$ > 0.4) with the isoprene nitrates type II factor.

*3.4.3. Isoprene Afternoon Factor.* The third isoprene factor, that we called isoprene afternoon, had a broad diurnal cycle with a maximum between 13:00 and 18:00, and virtually zero loading between 03:00 and 07:00 (Figure 4). The mass spectrum of the isoprene afternoon factor was largely dominated by $C_4$ and $C_5$ isoprene products in the series $C_4H_{4,6,8}O_{4,5}$ and $C_5H_{8,10,12}O_{4,5,6,8}$, the most abundant of which were $C_4H_6O_5$ ($m/z$ 196), $C_5H_6O_5$ ($m/z$ 208), $C_5H_8O_5$ ($m/z$ 210), and $C_5H_{10}O_5$ ($m/z$ 212). These ions, whose diurnal cycles are shown in Figure 8b, are the isoprene species forming from the photo-oxidation of ISOPOOH under low $NO_x$ that are observed to condense onto SOA particles.[20] Small quantities of isoprene ON ($C_5H_{9,11}NO_7$), which have a broad distribution extending well into the afternoon (Figure 8a) are also present. The time series in Figure 2f shows that OHR, had a good correlation with this factor, consistent with previous work showing that isoprene accounted for more than half of the total OHR during the day at the CTR site.[59,60] The correlation of this factor with external tracers (Figure 5f) was highest with $HO_2$, $O_3$, $HNO_3$, and solar radiation (Pearson $R$ > 0.5), consistent with its daytime formation.

**3.5. Additional Ion Families.** The mass spectra in Figure 3 show the significant presence of several compounds in the range $C_6$−$C_8$. In our PMF results, we found a strong $C_6H_{8,10}O_5$ signal in the isoprene afternoon factor and high levels of $C_7$ and $C_8$ compounds in both terpene (e.g., $C_7H_{10}O_4$, $C_8H_{12}O_4$, and $C_7H_9NO_6$) and isoprene (e.g., $C_7H_8O_5$, $C_7H_{10}O_5$, and $C_8H_{12}O_6$) PMF factors. $C_6$, $C_7$, and $C_8$ compounds have been found in both BVOC and anthropogenic VOC (AVOC) oxidation products. For instance, $C_7H_9NO_6$ has been detected in laboratory experiments on $\beta$-pinene + $NO_3$.[28] Ions in the


DOI: 10.1021/acsearthspacechem.8b00028
ACS Earth Space Chem. 2018, 2, 653−672

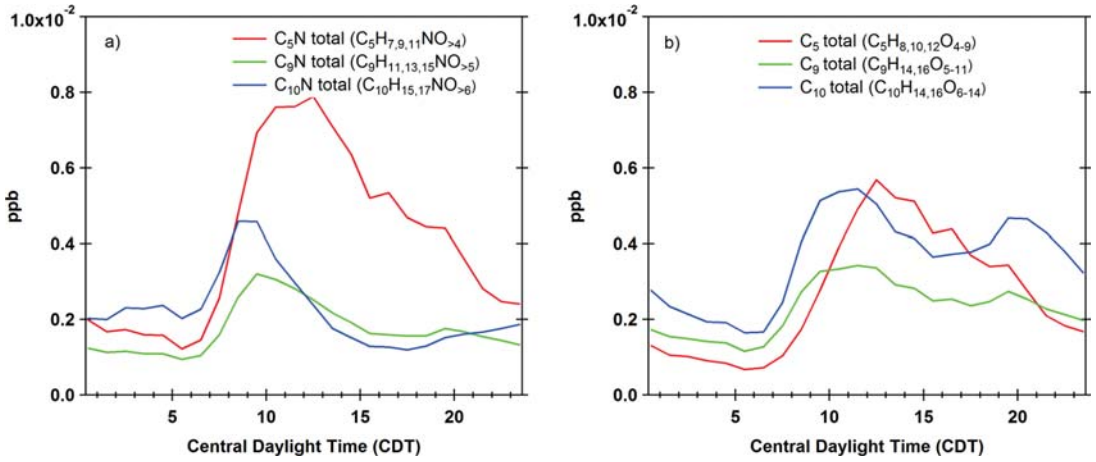


**Figure 9.** Diurnal cycles of (a) total $C_5N$, $C_9N$, and $C_{10}N$ ONs and (b) total $C_5$, $C_9$, and $C_{10}$ compounds. Each trace is the sum of 15−20 molecules, as indicated in the legend. Dinitrates were excluded. The total $C_5$ was comparable to the $C_{10}$ and $C_9$ amounts, whereas $C_5N$ was much higher than $C_9N$ and $C_{10}N$.

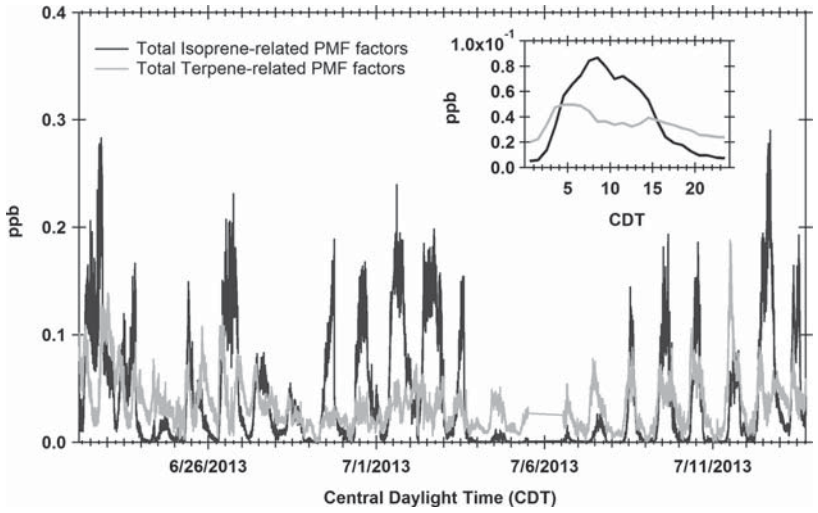


**Figure 10.** Time series of the $NO_3^-$ CIMS total terpene- and isoprene-related PMF factors along with their diurnal cycles (inset). The total terpene-related factor signal had small diurnal oscillations; the total isoprene-related factor signal reached a higher value during the day but collapsed to almost zero at night. The campaign-average mass loadings of total terpene- and isoprene-related factors were 0.03 and 0.04 ppb, respectively.

series $C_{6-9}H_{8,10,12,14}O_{6-12}$ were generated from the oxidation of $\alpha$-pinene at high $NO_x$ and low OH concentrations.[15] Finally, $C_7$ and $C_8$ compounds have been reported from the oxidation of terpenes in the laboratory and in ambient data from the boreal forest.[8,19] However, $C_6H_{8,10}O_{4-9}$ ions have also been detected following OH oxidation of benzene ($C_6H_6$).[61] Similarly, the molecules $C_7H_{10}O_5$ and $C_7H_{10}O_6$ have been detected in flow-tube laboratory studies of both myrcene ozonolysis[8] and toluene OH oxidation.[61] Finally, $C_8H_{12}O_6$ has been identified as the $\alpha$-pinene + OH reaction product 3-methyl-1,2,3-butanetricarboxylic acid (MBTCA),[62] but it also appears to be detected in the oxidation of ethylbenzene.[61] The CTR site was dominated by biogenic emissions, and therefore, we expected the majority of the observed ions to be of biogenic nature. However, there was a clear influence of anthropogenic air masses, as shown by the constant $NO_x$ presence and by the frequent $SO_2$ plumes. When looking at time series of all $C_6$−$C_8$ ions that have been identified from AVOC oxidation,[61] we did not find any particular trend different from the rest of the other biogenic products. We noticed only a similarity between temporal trends of gas-phase CO and the time series of $C_6H_8O_5$, $C_6H_8O_6$, and occasionally $C_7H_{10}O_5$, $C_8H_{10}O_5$, and $C_8H_{10}O_6$ (results not shown). Although not conclusive, we cannot exclude that a fraction of these molecules might have been of anthropogenic origin during particular time periods.

In regard to $C_n > 10$ products, several $C_{11}$ ions ($C_{11}H_{17}NO_{12,13,14}$) are present in the mass spectra of both terpene nitrates and isoprene nitrates type I factors. Compounds with similar molecular formulas ($C_{11}H_{19,21}NO_8$) in the particle phase were reported during SOAS by the colocated FIGAERO $I^-$ CIMS,[31] but their formation pathway has not been explained. We hypothesize that they correspond to products of $R'O_2 + R''O_2$ self-reactions, where the molecular compositions of R′ and R″ are unknown but sum to $C_{11}$ (e.g., $C_5 + C_6$). We also found several $C_{14}$ and $C_{15}$ species (e.g., $C_{15}H_{24}O_{8-11}$) in the mass spectra of all of the terpene factors as well as several $C_{14}$ and $C_{15}$ ONs, such as $C_{15}H_{25}NO_{6,7}$ and $C_{15}H_{23}NO_9$, in the terpene nitrates factor and $C_{14}H_{21}NO_{10}$ in the terpene nighttime factor. The diurnal profiles of the $C_{11}$ ONs (not shown) have a broad single peak in the morning


DOI: 10.1021/acsearthspacechem.8b00028
ACS Earth Space Chem. 2018, 2, 653−672

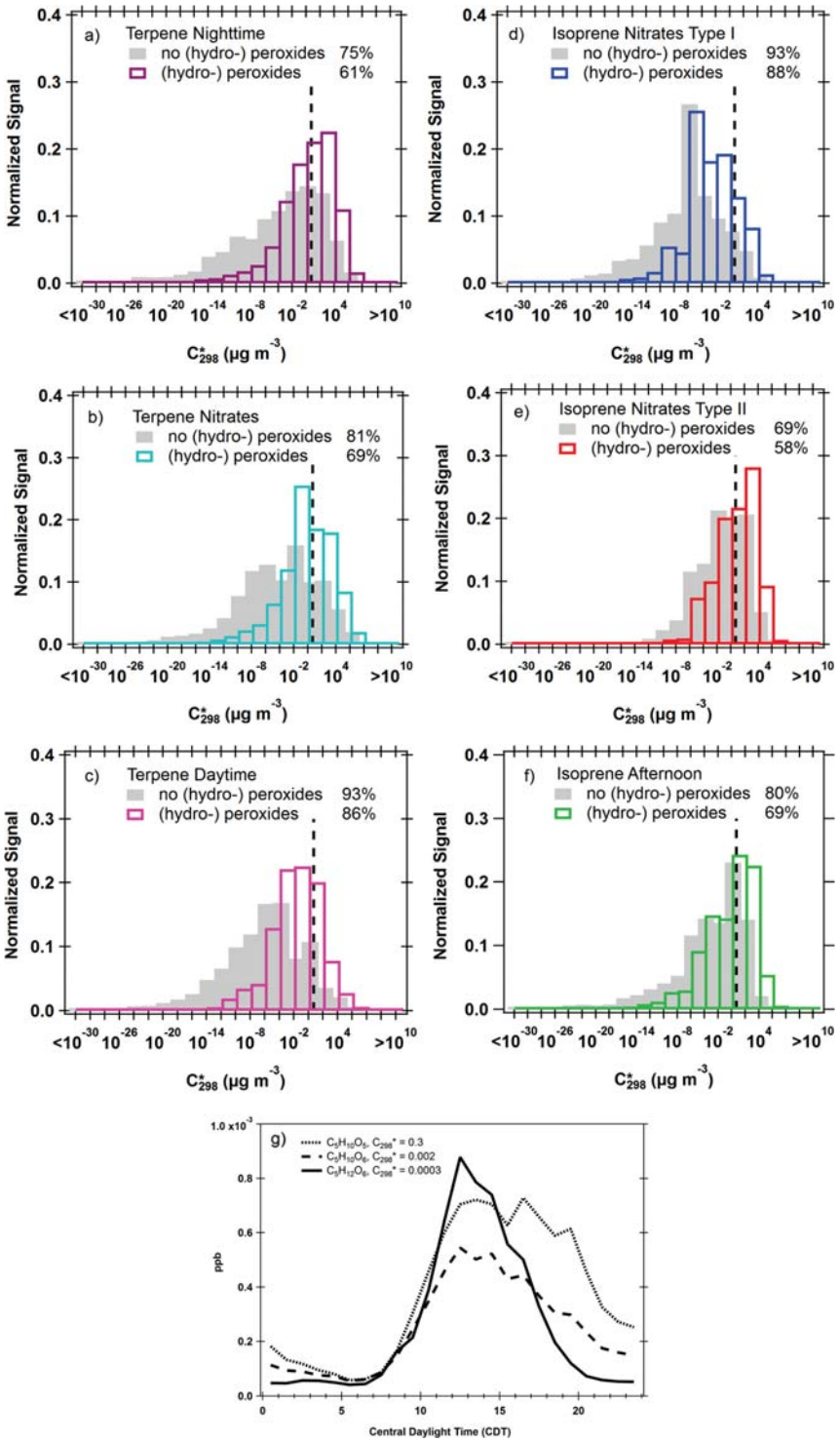


**Figure 11.** (a–f) Estimated volatilities ($C^*_{298}$, in $\mu$g m$^{-3}$) of the (a–c) terpene-related and (d–f) isoprene-related PMF factors calculated with and without assigning peroxy and hydroperoxy groups. The dashed lines separate the signals in the condensed phase (left) and gas phase (right). The percentage values refer to the fractions of signal in the particle phase. (g) Diurnal profiles of three ions with different $C^*_{298}$. The ion with the lowest $C^*_{298}$ ($C_5H_{12}O_6$, $C^*_{298}$ = 0.0003 $\mu$g m$^{-3}$) has a faster-decreasing profile than the ions with higher $C^*_{298}$. The ions are plotted with an offset in the *y* axis to align the starts of their diurnal cycles.

around 10:00–11:00 (perhaps explaining their presence in both the terpene nitrates and isoprene nitrates type I factors). The $C_{14}$ and $C_{15}$ ONs have a narrow, strong peak around 10:00 and a weaker peak at 20:00, while the $C_{14}$ and $C_{15}$ non-ON ions have a broad presence throughout the day, from 11:00 until late at night. $C_{15}$ ions have been reported at the CTR site both in the gas and particle phases and have been attributed to oxidation of sesquiterpenes,[31] which can be emitted by plants during both the day and night.[63] However, we cannot exclude



DOI: 10.1021/acsearthspacechem.8b00028
ACS Earth Space Chem. 2018, 2, 653–672

the role of $R'O_2$ + $R''O_2$ reactions or other chemical processes for $C_{15}$ formation as well.

## 4. DISCUSSION

**4.1. Summary of $NO_3^-$ CIMS PMF Analysis.** The results presented so far highlight the central role of nitrogen chemistry on BVOC oxidation during the SOAS 2013 campaign due to the constant presence of $NO_x$ at the site as shown by previous work.[21,25,26,31] Figure 9a shows the diurnal cycles of the total $C_5$ and $C_{10}$ ON compounds, which were obtained by adding the major identified ON molecules as listed in the legend (dinitrates were excluded). The isoprene ONs ($C_5N$) were much more abundant than the terpene ONs ($C_9N$ and $C_{10}N$). Figure 9b instead reports the sum of the identified $C_5$, $C_9$, and $C_{10}$ species. The $C_5$ compounds were about a third of the sum of the $C_9$ and $C_{10}$ species. The dominant signals for $C_5$ and $C_5N$ both peaked in the afternoon, coincident with OH chemistry. The $C_9N$ and $C_{10}N$ signals peaked in the morning around 08:00, while the $C_9$ and $C_{10}$ signals peaked at ∼10:00 and ∼20:00, likely reflecting formation from daytime photochemistry as well as ozonolysis. These results are consistent with the diurnal cycles of $C_5$ and $C_{10}$ particle ONs (pONs) measured by the colocated $I^-$ CIMS,[31] which showed that $C_5$ pONs peaked around 11:00 and stayed elevated in the afternoon while the $C_{10}$ pONs peaked at 08:00 and sharply decayed after 10:00.

The time series of the total terpene-related and isoprene-related factors, along with their diurnal cycles, are shown in Figure 10. Though both groups had a clear daily cycle, the diurnal variation of the total isoprene factors was more pronounced. The concentrations of the isoprene factors were larger than those of their monoterpene counterparts during the daytime; however, as noted earlier, the isoprene products go virtually to zero at night, while the terpene products always have a nonzero background. These observations are consistent with the fact that monoterpenes are emitted and can get oxidized during both the day and night (although $O_3$ and $NO_3$ radical oxidation in absence of sunlight seem to be preferred pathways and produce more HOMs) while isoprene emissions occur in the daytime and their chemistry is OH-initiated. It is also worth noting that the isoprene-related factors were almost zero during July 4−8, when rain, cloud cover, and lower solar radiation (Figure S10) might have suppressed the isoprene chemistry. However, the overall campaign-average mass loadings of total terpene- and total isoprene-derived factors were comparable (0.03 and 0.04 ppb, respectively). For completeness, the time series and diurnal cycles of the total monoterpene and isoprene precursors measured by the PTR-ToF-MS are reported in Figure S11. The isoprene precursor increases after 06:00 and reaches a maximum at 15:00, exhibiting a profile that is very similar to the isoprene afternoon PMF factor, while the monoterpene precursors have a maximum at night and a minimum during the day, similar to the terpene nighttime PMF factor.

Figure 11a−f shows the volatility profiles for all of the PMF factors expressed as normalized signal versus volatility ($C^*_{298}$, in $\mu g\ m^{-3}$) spanning from $10^{-30}$ to $>10^{10}$. Volatilities for individual formulas (excluding the $NO_3^-$ clustering ion) were calculated from a model based on SIMPOL, a simple group contribution method for predicting vapor pressures and enthalpies of vaporization of multifunctional organic compounds.[64] A constant temperature of 298 K, equal to the average campaign temperature of 25 °C during SOAS 2013, was used in the model. The fraction in the particle phase ($F_p$) was calculated from $C^*_{298}$ and OA via the expression

$$F_p = \left(\frac{C^*_{298}}{OA} + 1\right)^{-1} \quad (3)$$

where the OA was taken from the colocated HR-AMS[23] and averaged 7.5 ± 5.3 $\mu g\ m^{-3}$. We investigated two different methods for assigning functional groups from chemical formulas. Both methods use a combination of rings plus double-bond equivalents (RPDBE) and elemental numbers to constrain possible functional groups. The first method assigns all RPDBE to carbonyl groups.[65,66] If not enough oxygen atoms are present, C=C double bonds are assigned unless $C_n > 10$, in which case one unit of RPDBE is also assumed to be due to a carbon ring structure or an epoxide. If enough oxygen atoms are present, the excess oxygen is assigned to hydroxyl groups. Then the hydroxyl and carbonyl groups are combined to two carboxyl groups at most. A second method, developed specifically for this study, provides an estimate of the maximum numbers of peroxy and hydroperoxy groups, which are common functional groups in BVOC oxidation from both isoprene and monoterpene oxidation, that could be assigned to a given molecular formula.[5,20,31] As in the previous method, all RPDBE are first assigned to carbonyl groups involving all available oxygen atoms, and the remaining RPDBE are assigned to C=C double bonds and/or carbon ring structures depending on the number of oxygen atoms. For formulas that contains 13 or more carbon atoms, oxygen atoms that remain after RPDBE assignments are assigned to one peroxy (R−OO−R′) group, mimicking the formation of oligomers. Additional oxygen atoms are assigned to hydroperoxy groups (−OOH), and any oxygen left is assigned to a hydroxyl group. The inclusion of peroxy and hydroperoxy groups leads to increased volatility for many formulas, sometimes up to 10 orders of magnitude higher compared with the first method. While the exact functional group distribution for compounds measured during SOAS 2013 is unknown, the first method is likely to produce a lower limit for the volatility, since it has as many hydroxyl groups per molecule as possible and those groups are the most efficient (per oxygen atom) at reducing vapor pressure. The second method including the peroxy and hydroperoxy groups might constitute an upper limit for volatility since that method maximizes the number of peroxy groups, which are less efficient (per oxygen atom) at reducing the vapor pressure.

Volatility distributions obtained using both methods for (a−c) the terpene-related factors and (d−f) the isoprene-related factors are compared in Figure 11. Overall, we expect species with low $C^*_{298}$ to have short lifetimes and disappear from the gas phase (by condensing onto particles) when they stop being produced and the species with high $C^*_{298}$ to stay in the gas phase for much longer (until they are lost to further oxidation or dry deposition). Most of the signal shown in all of the factor volatility distributions is below the dashed line ($C^*_{298}$= 7.5 mg $m^{-3}$) in both cases, i.e., with and without inclusion of peroxy and hydroperoxy groups. This result is consistent with the $NO_3^-$ CIMS being selective toward compounds that are expected to irreversibly condense onto the particle phase upon collision because of their low volatility and the high accommodation coefficients for oxidized organics.[5,20,67,68] However, when peroxy and hydroperoxy groups are included, the fraction of signal that is in the particle phase (under


DOI: 10.1021/acsearthspacechem.8b00028
ACS Earth Space Chem. 2018, 2, 653−672

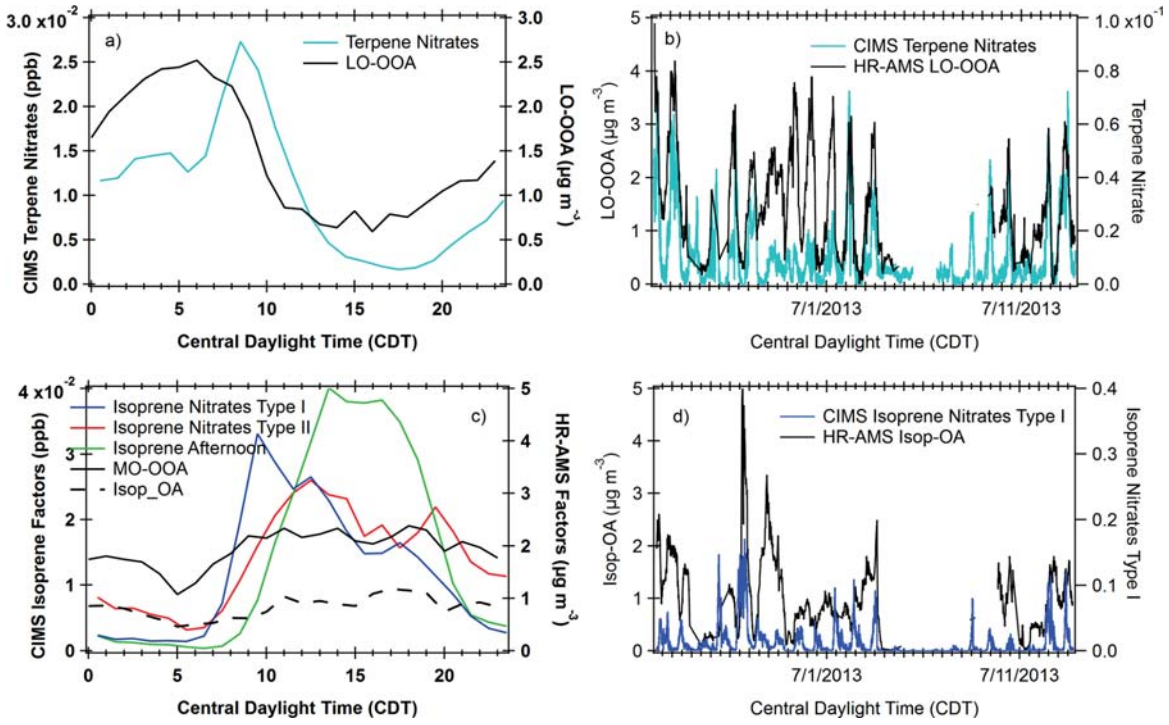


**Figure 12.** Comparison between PMF factors from the $NO_3^-$ CIMS (colored traces) and the colocated HR-AMS (black solid and dashed traces): (a, c) diurnal cycle comparisons; (b, d) time series of selected factors.

equilibrium) is reduced. In addition, the volatility distributions estimated for structures that include peroxy and hydroperoxy groups peak much closer to the dashed line compared with the ones obtained with the original method (this is especially true for the terpene daytime and isoprene nitrate type I factors in Figure 11c,d, respectively). The diurnal cycles of the various oxidation products should also reflect their different estimated volatilities, as ions with low $C^*_{298}$ are expected to have a faster-decreasing diurnal profile than ions with higher $C^*_{298}$. To illustrate this, Figure 11g shows the diurnal profiles of $C_5H_{10}O_6$, $C_5H_{10}O_6$, and $C_5H_{12}O_6$, three species found in the same factor (isoprene afternoon), which suggests production from the same source. The three ions overlap at the start of the day but decay differently. Consistent with the calculated volatilities, we find that the ion with the highest $C^*_{298}$ ($C_5H_{10}O_5$, $C^*_{298}$ = 0.3) has the slowest decay, indicating a long-lasting presence in the gas phase, while $C_5H_{12}O_6$ ($C^*_{298}$ = 0.0003) has a faster decay, i.e., possibly condensing faster onto the particle phase.

**4.2. Comparison with HR-AMS PMF Analysis.** This section discusses the comparison between the PMF factors obtained from the analysis of the $NO_3^-$ CIMS data and the ones reported for a colocated HR-AMS.[23] The aim of such a comparison, which has not been carried out systematically before, is to evaluate the existence of any relationship between the gas and particle phases. As previously stated, many of the gas-phase ONs observed by the $NO_3^-$ CIMS were found in the particle phase detected by the colocated $I^-$ CIMS.[31] In addition, the volatility distributions showed that a large fraction of the PMF factors' signal is expected to condense on the particle phase. However, we do not expect matching profiles for the HR-AMS and CIMS PMF factors because of the inherent differences in partitioning time scales between gaseous and particle species, i.e., the low-volatility gas-phase species represent a snapshot of the last minutes of reactive chemistry, while the aerosol serves as an "integrator" of such signals over periods of days. Figure 12 shows the comparison of diurnal cycles and selected time series for CIMS and HR-AMS PMF factors. We find that the profile of the HR-AMS less oxygenated organic aerosol (LO-OOA), which was explained by monoterpene oxidation via $NO_3$ radical chemistry,[23] has a diurnal cycle that is similar to the CIMS terpene nitrates factor, although the LO-OOA peaks earlier than the terpene nitrates (Figure 12a). Additional data sets collected in the southeast U.S. have shown that the LO-OOA factor correlates well with measurements of AMS particle ONs,[26] whose diurnal cycles show a maximum between 07:00 and 09:00, thus closer to the peak of the CIMS terpene nitrates diurnal cycle. This suggests that particle-phase ONs within the LO-OOA AMS factor were likely formed by condensation of low-volatility gas-phase ONs. The time series of the HR-AMS LO-OOA and CIMS terpene nitrates are reported in Figure 12b, where a varying degree of similarity between profiles can be observed. Figure 12c shows instead the diurnal profiles of the HR-AMS more oxygenated organic aerosol (MO-OOA) and Isop-OA (an isoprene SOA formed via reactive uptake of epoxydiols, IEPOX[24]) along with the diurnal profiles for all of the $NO_3^-$ CIMS isoprene-related factors. Both MO-OOA and Isop-OA have much broader diurnal profiles that the CIMS isoprene-related factors. Figure 12d shows a strong correlation between the isoprene nitrates type I factor and the Isop-OA factor during the high-$SO_2$ event of June 27. This is consistent with Isop-OA formation being directly mediated by the amount of particle $SO_4$, indicating a strong link with sulfate-rich plumes.[23] The HR-AMS MO-OOA factor, which is interpreted as highly aged OA,[26] is most strongly correlated with the isoprene nitrates type II factor. It is therefore possible that both ONs and some of the condensing isoprene species[20] forming in the late afternoon contributed to


DOI: 10.1021/acsearthspacechem.8b00028
ACS Earth Space Chem. 2018, 2, 653−672

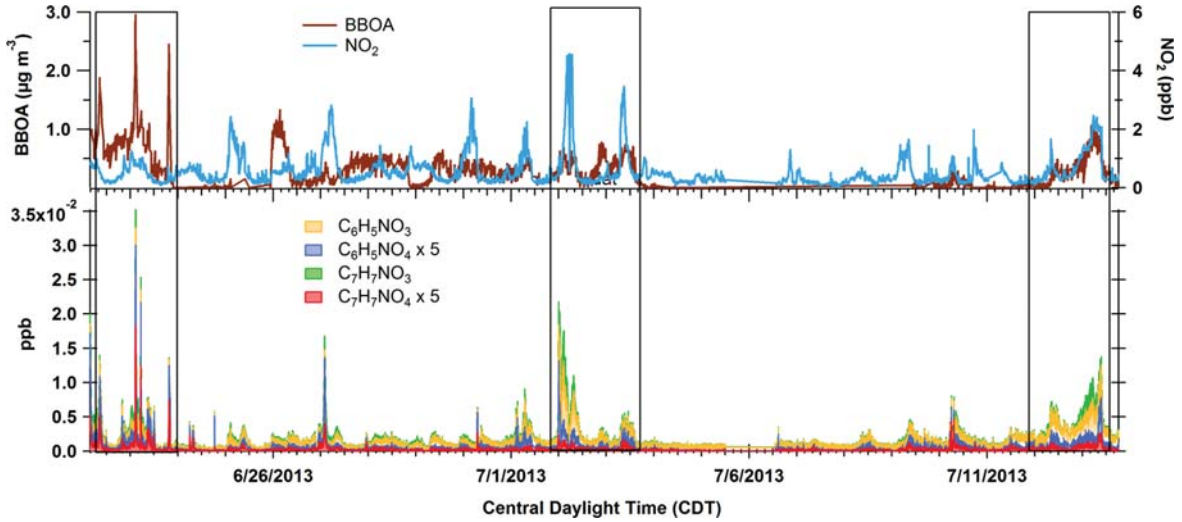


**Figure 13.** Time series of $C_6$ and $C_7$ gas-phase ions corresponding to the formulas of phenolic species measured by the $NO_3^-$ CIMS during SOAS 2013. These species were sporadically elevated during events associated with biomass burning. The solid boxes highlight the times where phenol enhancements correlated clearly with both the HR-AMS BBOA factor and gas-phase $NO_2$. The clustering reagent ion $NO_3^-$ has been omitted from the formulas to make the labels more readable.

this particle OA component, for which no specific source was originally identified.[23]

The HR-AMS PMF analysis also reported a biomass-burning organic aerosol (BBOA) factor contributing about 10% of the OA mass.[23] The $NO_3^-$ CIMS detected several elemental formulas that have been previously associated with phenolic compounds in biomass-burning emissions, including $C_6H_5NO_3$ (formula of nitrophenol), $C_6H_5NO_4$ (nitrocatechol), $C_7H_7NO_3$ (methylnitrophenol), and $C_7H_7NO_4$ (methylnitrocatechol).[69] Throughout the SOAS 2013 campaign, these species were sometimes correlated with both the HR-AMS BBOA factor and $NO_2$ traces, as shown in Figure 13. At other times, they displayed only a correlation with $NO_2$ and not with the BBOA factor or vice versa, indicating decoupled sources of BBOA and $NO_2$ and possibly several sources for these molecules other than biomass burning (or isomeric forms of these compounds associated with different sources). The "phenolic" species were not included in the PMF presented here because they could not be isolated in a specific factor even when more solutions were explored ($p > 8$), likely because of their sporadic occurrence throughout the campaign. It is worth noting that a factor exclusively dominated by $C_6H_5NO_3$ was also reported in the PMF of the Hyytiälä data.[19] This factor was explained by long-range transport of biomass-burning plumes from Eastern Europe and appeared as a constant background, making it easier to isolate via PMF.

## 5. CONCLUSIONS

We have presented $NO_3^-$ CIMS measurements obtained at the CTR forest site during SOAS 2013. The results reported here represent the first ambient measurements with a $NO_3^-$ CIMS in an isoprene-dominated environment. We identified several hundred ion formulas consistent with oxidation products of both isoprene and terpenes and many other compounds with carbon numbers ranging from $C_3$ to $C_{20}$. Organic nitrates (ONs) were a significant component of the $NO_3^-$ CIMS spectra and were found throughout the day, reflecting daytime and nighttime formation pathways. PMF analysis was applied to deconvolve the complexity of the data set, and it resolved six primary factors, three isoprene-related and three terpene-related, all of them influenced in different ways by anthropogenic emissions. The campaign-average mixing ratio contributions of the six factors varied between 14% and 19%. Each of the PMF factors had a characteristic diurnal cycle that could be explained by a primary chemical pathway. The terpene factor with a nighttime peak had the majority of $\alpha$-pinene highly oxidized molecules (HOMs), consistent with monoterpene ozonolysis. However, some nitrogen-containing compounds were also found at night, reflecting $NO_3$ radical oxidation chemistry. The other two terpene factors were higher during the daytime. The terpene nitrates factor contained mostly ON and peaked in the early morning hours after the NO daily maximum, indicating the relevance of $RO_2$ + NO radical termination reactions; however, the elevated concentrations of $C_{10}H_{17}NO_{6-10}$ ions in this factor before sunrise suggested a contribution from $NO_3$-initiated oxidation processes. The terpene daytime factor peaked around midday and was characterized by $C_5$ fragments, likely formed from the OH oxidation of monoterpenes. The isoprene-related factors were highest during the daytime, even though the isoprene nitrates type II factor had a second diurnal peak right after sunset. The non-nitrogen-containing isoprene products were mostly concentrated in the isoprene afternoon factor. Finally, we found an isoprene nitrates type I factor that correlated with the $SO_2$ plumes occasionally reaching the CTR site and was dominated by an isoprene-derived dinitrate ($C_5H_{10}N_2O_8$). Consistent with previous work, the $NO_3^-$ CIMS data set revealed the importance of nitrogen chemistry for the formation of highly oxidized molecules, especially for isoprene: in fact, isoprene organonitrates ($C_5N$) were more abundant than the monoterpene counterparts ($C_9N$ and $C_{10}N$) and more abundant than the $C_5$ products. The diurnal cycles of the ions identified from high-resolution analysis were highly variable, reflecting the diverse chemical processes involved in the formation of atmospheric oxidized molecules in the gas phase. Subgroups of ions with similar diurnal trends helped with interpretation of the PMF factors. These results indicate


DOI: 10.1021/acsearthspacechem.8b00028
ACS Earth Space Chem. 2018, 2, 653−672

the overall usefulness of PMF analysis to understand and interpret complex mass spectrometry of ambient data sets.

## ■ ASSOCIATED CONTENT

### Supporting Information

The Supporting Information is available free of charge on the ACS Publications website at DOI: 10.1021/acsearthspacechem.8b00028.

Relative ion transmission measurement method (section 1); PMF analysis error calculations and diagnostics (section 2); transmission measurement results (Figure S1); campaign-average high-resolution mass spectrum and example of high-resolution fit (Figure S2); effects of changes in humidity and pressure in the SSQ on nitrate reagent ions (Figure S3); PMF diagnostics and PMF mass spectra for the six-factor solution (Figure S4); source allocation from two- to 10-factor PMF solutions (Figure S5); approximate $OS_c$ as a function of $C_n$ and normalized factor signal as a function of $OS_c$ for each PMF factor (Figure S6); diurnal cycles of isoprene dinitrate and monoterpene dinitrate ions along with high-resolution fits of two $m/z$ where dinitrate ions are detected (Figure S7); FLEXPART back-trajectories of the air masses during high $SO_2$ events (Figure S8); map of the state of Alabama and location of the major coal-fired power plants (Figure S9); temporal series of temperature, relative humidity, and solar radiation at the CTR site (Figure S10); time series and diurnal cycles of the monoterpene and isoprene precursors as measured by PTR-ToF-MS (Figure S11) (PDF)

## ■ AUTHOR INFORMATION


### Corresponding Author

*E-mail: pmassoli@aerodyne.com.

### ORCID

Paola Massoli: 0000-0002-6378-9366
Harald Stark: 0000-0002-0731-1202
Jordan E. Krechmer: 0000-0003-3642-0659
Lu Xu: 0000-0002-0021-9876
Nga L. Ng: 0000-0001-8460-4765
Pawel K. Misztal: 0000-0003-1060-1750
Jose L. Jimenez: 0000-0001-6203-1847

### Present Addresses

▲L.X.: Division of Geological and Planetary Sciences, California Institute of Technology, Pasadena, CA 91125, United States.

∞Centre for Ecology, Hydrology Edinburgh, Midlothian, EH26 0QB, UK.


### Notes

This paper has not been formally reviewed by the funding agencies. The views expressed in this document are solely those of the authors and do not necessarily reflect those of the funding agencies.

The authors declare no competing financial interest.

The $NO_3^-$ CIMS data are available upon request from the corresponding author (pmassoli@aerodyne.com).

## ■ ACKNOWLEDGMENTS

The authors thank the organizers of the SOAS campaign for their assistance and help during the project at the CTR site, Andrew T. Lambe (Aerodyne Research), Heikki Junninen, Mikael Ehn, Mikko Sipila, and Jani Hakala (University of Helsinki) for their help before and during the project and for the useful comments, Karsten Bauman and Eric Edgerton (ARA) for sharing the SEARCH data, Steven Bertram and Paul Shepson (Western Michigan University) for sharing the 2D-GC and GC-ECD data, and William Brune (Pennsylvania State University) for sharing the $HO_2$, OH, and OHR data. Christopher Knote (NCAR) produced the FLEXPART outputs during the SOAS project. This project was funded by NSF AGS-1243356. L.X. and N.L.N. acknowledge support from NSF AGS-1242258 and U.S. EPA STAR 83540301. J.E.K. and J.L.J. were supported by NSF AGS-1740610 and U.S. EPA STAR 83587701.

## ■ REFERENCES


(1) Kimmel, J. R.; Farmer, D. K.; Cubison, M. J.; Sueper, D.; Tanner, C.; Nemitz, E.; Worsnop, D. R.; Gonin, M.; Jimenez, J. L. Real-time aerosol mass spectrometry with millisecond resolution. *Int. J. Mass Spectrom.* **2011**, *303* (1), 15−26.

(2) Yatavelli, R. L. N.; Lopez-Hilfiker, F. D.; Wargo, J. D.; Kimmel, J. R.; Cubison, M. J.; Bertram, T. H.; Jimenez, J.-L.; Gonin, M.; Worsnop, D. R.; Thornton, J. A. Chemical Ionization High-Resolution Time-of-Flight Mass Spectrometer Coupled to a Micro Orifice Volatilization Impactor (MOVI-HRToF-CIMS) for Analysis of Gas and Particle-Phase Organic Species. *Aerosol Sci. Technol.* **2012**, *46*, 1313−1327.

(3) Ehn, M.; Junninen, H.; Petäjä, T.; Kurtén, T.; Kerminen, V.-M.; Schobesberger, S.; Manninen, H. E.; Ortega, I. K.; Vehkamäki, H.; Kulmala, M.; Worsnop, D. R. Composition and temporal behavior of ambient ions in the boreal forest. *Atmos. Chem. Phys.* **2010**, *10*, 8513−8530.

(4) Ehn, M.; Kleist, E.; Junninen, H.; Petäjä, T.; Lönn, G.; Schobesberger, S.; Dal Maso, M.; Trimborn, A.; Kulmala, M.; Worsnop, D. R.; Wahner, A.; Wildt, J.; Mentel, T. F. Gas phase formation of extremely oxidized pinene reaction products in chamber and ambient air. *Atmos. Chem. Phys.* **2012**, *12*, 5113−5127.

(5) Ehn, M.; Thornton, J. A.; Kleist, E.; Sipilä, M.; Junninen, H.; Pullinen, I.; Springer, M.; Rubach, F.; Tillmann, R.; Lee, B. H.; Lopez-Hilfiker, F. D.; Andres, S.; Acir, I. H.; Rissanen, M.; Jokinen, T.; Schobesberger, S.; Kangasluoma, J.; Kontkanen, J.; Nieminen, T.; Kurtén, T.; Nielsen, L. B.; Jorgensen, S.; Kjaergaard, H. G.; Canagaratna, M.; Dal Maso, M.; Berndt, T.; Petäjä, T.; Wahner, A.; Kerminen, V.-M.; Kulmala, M.; Worsnop, D. R.; Wildt, J.; Mentel, T. F. A large source of low-volatility secondary organic aerosol. *Nature* **2014**, *506* (7489), 476−479.

(6) Schobesberger, S.; Franchin, A.; Bianchi, F.; Rondo, L.; Duplissy, J.; Kürten, A.; Ortega, I. K.; Metzger, A.; Schnitzhofer, R.; Almeida, J.; Amorim, A.; Dommen, J.; Dunne, E. M.; Ehn, M.; Gagné, S.; Ickes, L.; Junninen, H.; Hansel, A.; Kerminen, V.-M.; Kirkby, J.; Kupc, A.; Laaksonen, A.; Lehtipalo, K.; Mathot, S.; Onnela, A.; Petäjä, T.; Riccobono, F.; Santos, F. D.; Sipilä, M.; Tomé, A.; Tsagkogeorgas, G.; Viisanen, Y.; Wagner, P. E.; Wimmer, D.; Curtius, J.; Donahue, N. M.; Baltensperger, U.; Kulmala, M.; Worsnop, D. R. On the composition of ammonia−sulfuric-acid ion clusters during aerosol particle formation. *Atmos. Chem. Phys.* **2015**, *15*, 55−78.

(7) Riccobono, F.; Schobesberger, S.; Scott, C. E.; Dommen, J.; Ortega, I. K.; Rondo, L.; Almeida, J.; Amorim, A.; Bianchi, F.; Breitenlechner, M.; David, A.; Downard, A.; Dunne, E.; Duplissy, J.; Ehrhart, S.; Flagan, R. C.; Franchin, A.; Hansel, A.; Junninen, H.; Kajos, M.; Keskinen, H.; Kupc, A.; Kürten, A.; Kvashin, A. N.; Laaksonen, A.; Lehtipalo, K.; Makhmutov, V.; Mathot, S.; Nieminen, T.; Onnela, A.; Petäjä, T.; Praplan, A. P.; Santos, F. D.; Schallhart, S.; Seinfeld, J. H.; Sipilä, M.; Spracklen, D. V.; Stozhkov, Y.; Stratmann, F.; Tomé, A.; Tsagkogeorgas, G.; Vaattovaara, P.; Viisanen, Y.; Vrtala, A.; Wagner, P. E.; Weingartner, E.; Wex, H.; Wimmer, D.; Carslaw, K. S.; Curtius, J.; Donahue, N. M.; Kirkby, J.; Kulmala, M.; Worsnop, D. R.; Baltensperger, U. Oxidation Products of Biogenic Emissions




DOI: 10.1021/acsearthspacechem.8b00028
ACS Earth Space Chem. 2018, 2, 653−672

Contribute to Nucleation of Atmospheric Particles. *Science* **2014**, *344* (6185), 717−721.
(8) Jokinen, T.; Berndt, T.; Makkonen, R.; Kerminen, V. M.; Junninen, H.; Paasonen, P.; Stratmann, F.; Herrmann, H.; Guenther, A. B.; Worsnop, D. R.; Kulmala, M.; Ehn, M.; Sipilä, M. Production of extremely low volatile organic compounds from biogenic emissions: Measured yields and atmospheric implications. *Proc. Natl. Acad. Sci. U. S. A.* **2015**, *112* (23), 7123−7128.
(9) Bianchi, F.; Tröstl, J.; Junninen, H.; Frege, C.; Henne, S.; Hoyle, C. R.; Molteni, U.; Herrmann, E.; Adamov, A.; Bukowiecki, N.; Chen, X.; Duplissy, J.; Gysel, M.; Hutterli, M.; Kangasluoma, J.; Kontkanen, J.; Kürten, A.; Manninen, H. E.; Münch, S.; Peräkylä, O.; Petäjä, T.; Rondo, L.; Williamson, C.; Weingartner, E.; Curtius, J.; Worsnop, D. R.; Kulmala, M.; Dommen, J.; Baltensperger, U. New particle formation in the free troposphere: A question of chemistry and timing. *Science* **2016**, *352* (6289), 1109−1112.
(10) Aljawhary, D.; Lee, A. K. Y.; Abbatt, J. P. D. High-resolution chemical ionization mass spectrometry (ToF-CIMS): application to study SOA composition and processing. *Atmos. Meas. Tech.* **2013**, *6*, 3211−3224.
(11) Guenther, A. B.; Jiang, X.; Heald, C. L.; Sakulyanontvittaya, T.; Duhl, T.; Emmons, L. K.; Wang, X. The Model of Emissions of Gases and Aerosols from Nature version 2.1 (MEGAN2.1): an extended and updated framework for modeling biogenic emissions. *Geosci. Model Dev.* **2012**, *5*, 1471−1492.
(12) Carlton, A. G.; Wiedinmyer, C.; Kroll, J. H. A review of Secondary Organic Aerosol (SOA) formation from isoprene. *Atmos. Chem. Phys.* **2009**, *9*, 4987−5005.
(13) Rissanen, M. P.; Kurtén, T.; Sipilä, M.; Thornton, J. A.; Kangasluoma, J.; Sarnela, N.; Junninen, H.; Jørgensen, S.; Schallhart, S.; Kajos, M. K.; Taipale, R.; Springer, M.; Mentel, T. F.; Ruuskanen, T.; Petäjä, T.; Worsnop, D. R.; Kjaergaard, H. G.; Ehn, M. The Formation of Highly Oxidized Multifunctional Products in the Ozonolysis of Cyclohexene. *J. Am. Chem. Soc.* **2014**, *136* (44), 15596−15606.
(14) Mentel, T. F.; Springer, M.; Ehn, M.; Kleist, E.; Pullinen, I.; Kurtén, T.; Rissanen, M.; Wahner, A.; Wildt, J. Formation of highly oxidized multifunctional compounds: autoxidation of peroxy radicals formed in the ozonolysis of alkenes − deduced from structure−product relationships. *Atmos. Chem. Phys.* **2015**, *15*, 6745−6765.
(15) Lambe, A.; Massoli, P.; Zhang, X.; Canagaratna, M.; Nowak, J.; Daube, C.; Yan, C.; Nie, W.; Onasch, T.; Jayne, J.; Kolb, C.; Davidovits, P.; Worsnop, D.; Brune, W. H. Controlled nitric oxide production via $O(^1D)$ + $N_2O$ reactions for use in oxidation flow reactor studies. *Atmos. Meas. Tech.* **2017**, *10*, 2283−2298.
(16) Jokinen, T.; Sipilä, M.; Junninen, H.; Ehn, M.; Lönn, G.; Hakala, J.; Petäjä, T.; Mauldin, R. L., III; Kulmala, M.; Worsnop, D. R. Atmospheric sulphuric acid and neutral cluster measurements using CI-APi-TOF. *Atmos. Chem. Phys.* **2012**, *12*, 4117−4125.
(17) Eisele, F. L.; Tanner, D. J. Measurement of the gas phase concentration of $H_2SO_4$ and methane sulfonic acid and estimates of $H_2SO_4$ production and loss in the atmosphere. *J. Geophys. Res. Atmos* **1993**, *98* (D5), 9001−9010.
(18) Junninen, H.; Ehn, M.; Petäjä, T.; Luosujärvi, L.; Kotiaho, T.; Kostiainen, R.; Rohner, U.; Gonin, M.; Fuhrer, K.; Kulmala, M.; Worsnop, D. R. A high-resolution mass spectrometer to measure atmospheric ion composition. *Atmos. Meas. Tech.* **2010**, *3*, 1039−1053.
(19) Yan, C.; Nie, W.; Äijälä, M.; Rissanen, M. P.; Canagaratna, M. R.; Massoli, P.; Junninen, H.; Jokinen, T.; Sarnela, N.; Häme, S. A. K.; Schobesberger, S.; Canonaco, F.; Yao, L.; Prévôt, A. S. H.; Petäjä, T.; Kulmala, M.; Sipilä, M.; Worsnop, D. R.; Ehn, M. Source characterization of highly oxidized multifunctional compounds in a boreal forest environment using positive matrix factorization. *Atmos. Chem. Phys.* **2016**, *16*, 12715−12731.
(20) Krechmer, J.; Coggon, M. M.; Massoli, P.; Nguyen, T. B.; Crounse, J. D.; Hu, W.; Day, D. A.; Tyndall, G. S.; Henze, D. K.; Rivera-Rios, J. C.; Nowak, J. B.; Kimmel, J. R.; Mauldin, R. L., III; Stark, H.; Jayne, J. T.; Sipilä, M.; Junninen, H.; St. Clair, J. M.; Zhang, X.; Feiner, P. A.; Zhang, L.; Miller, D. O.; Brune, W. H.; Keutsch, F. N.; Wennberg, P. O.; Seinfeld, J. H.; Worsnop, D. R.; Jimenez, J.-L.; Canagaratna, M. R. Formation of low volatility organic compounds and secondary organic aerosol from isoprene hydroxyhydroperoxide low-NO oxidation. *Environ. Sci. Technol.* **2015**, *49* (17), 10330−10339.
(21) Carlton, A. M.; de Gouw, J.; Jimenez, J.-L.; Ambrose, J. L.; Attwood, A. R.; Brown, S.; Baker, K. R.; Brock, C. A.; Cohen, R. C.; Edgerton, S.; Farkas, C.; Farmer, D.; Goldstein, A. H.; Gratz, L.; Guenther, A.; Hunt, S.; Jaeglé, L.; Jaffe, D. A.; Mak, J.; McClure, C.; Nenes, A.; Nguyen, T. K. V.; Pierce, J. R.; de Sa, S.; Selin, N.; Shah, V.; Shaw, S.; Shepson, P. B.; Song, S.; Stutz, J.; Surratt, J.; Turpin, B. J.; Warneke, C.; Washenfelder, R. A.; Wennberg, P. O.; Zhou, X. The Southeast Atmosphere Studies (SAS): coordinated investigation and discovery to answer critical questions about fundamental atmospheric processes. *Bull. Am. Meteorol. Soc.* **2018**, *99* (3), 547−567.
(22) Hidy, G. M.; Blanchard, C. L.; Baumann, K.; Edgerton, E.; Tanenbaum, S.; Shaw, S.; Knipping, E.; Tombach, I.; Jansen, J.; Walters, J. Chemical climatology of the southeastern United States, 1999−2013. *Atmos. Chem. Phys.* **2014**, *14*, 11893−11914.
(23) Xu, L.; Guo, H.; Boyd, C.; Klein, M.; Bougiatioti, A.; Cerully, K.; Hite, J. R.; Isaacman-VanWertz, G.; Kreisberg, N.; Knote, C.; Olson, K.; Koss, A. R.; Goldstein, A. H.; Hering, S. V.; de Gouw, J. A.; Baumann, K.; Lee, S. H.; Nenes, A.; Weber, R. J.; Ng, N. L. Effects of Anthropogenic Emissions on Aerosol Formation from Isoprene and Monoterpenes in the Southeastern United States. *Proc. Natl. Acad. Sci. U. S. A.* **2015**, *112*, 37−42.
(24) Hu, W.; Campuzano-Jost, P.; Palm, B. B.; Day, D. A.; Ortega, A. M.; Hayes, P. L.; Krechmer, J. E.; Chen, Q.; Kuwata, M.; Liu, Y. J.; de Sá, S. S.; McKinney, K.; Martin, S. T.; Hu, M.; Budisulistiorini, S. H.; Riva, M.; Surratt, J. D.; St. Clair, J. M.; Isaacman-Van Wertz, G.; Yee, L. D.; Goldstein, A. H.; Carbone, S.; Brito, J.; Artaxo, P.; de Gouw, J. A.; Koss, A.; Wisthaler, A.; Mikoviny, T.; Karl, T.; Kaser, L.; Jud, W.; Hansel, A.; Docherty, K. S.; Alexander, M. L.; Robinson, N. H.; Coe, H.; Allan, J. D.; Canagaratna, M. R.; Paulot, F.; Jimenez, J.-L. Characterization of a real-time tracer for isoprene epoxydiols-derived secondary organic aerosol (IEPOX-SOA) from aerosol mass spectrometer measurements. *Atmos. Chem. Phys.* **2015**, *15*, 11807−11833.
(25) Ayres, B. R.; Allen, H. M.; Draper, D. C.; Brown, S. S.; Wild, R. J.; Jimenez, J. L.; Day, D. A.; Campuzano-Jost, P.; Hu, W.; de Gouw, J.; Koss, A.; Cohen, R. C.; Duffey, K. C.; Romer, P.; Baumann, K.; Edgerton, E.; Takahama, S.; Thornton, J. A.; Lee, B. H.; Lopez-Hilfiker, F. D.; Mohr, C.; Wennberg, P. O.; Nguyen, T. B.; Teng, A.; Goldstein, A. H.; Olson, K.; Fry, J. L. Organic nitrate aerosol formation via $NO_3$ + biogenic volatile organic compounds in the southeastern United States. *Atmos. Chem. Phys.* **2015**, *15*, 13377−13392.
(26) Xu, L.; Suresh, S.; Guo, H.; Weber, R. J.; Ng, N. L. Aerosol characterization over the southeastern United States using high-resolution aerosol mass spectrometry: spatial and seasonal variation of aerosol composition and sources with a focus on organic nitrates. *Atmos. Chem. Phys.* **2015**, *15*, 7307−7336.
(27) Boyd, C. M.; Sanchez, J.; Xu, L.; Eugene, A. J.; Nah, T.; Tuet, W. Y.; Guzman, M. I.; Ng, N. L. Secondary organic aerosol formation from the $\beta$-pinene+$NO_3$ system: effect of humidity and peroxy radical fate. *Atmos. Chem. Phys.* **2015**, *15*, 7497−7522.
(28) Nah, T.; Sanchez, J.; Boyd, C. M.; Ng, N. L. Photochemical aging of $\alpha$-pinene and $\beta$-pinene secondary organic aerosol formed from nitrate radical oxidation. *Environ. Sci. Technol.* **2016**, *50*, 222−231.
(29) Nguyen, T. B.; Crounse, J. D.; Teng, A. P.; St. Clair, J. M.; Paulot, F.; Wolfe, G. M.; Wennberg, P. O. Rapid deposition of oxidized biogenic compounds to a temperate forest. *Proc. Natl. Acad. Sci. U. S. A.* **2015**, *112* (5), E392−E401.
(30) Xiong, F.; McAvey, K. M.; Pratt, K. A.; Groff, C. J.; Hostetler, M. A.; Lipton, M. A.; Starn, T. K.; Seeley, J. V.; Bertman, S. B.; Teng, A. P.; Crounse, J. D.; Nguyen, T. B.; Wennberg, P. O.; Misztal, P. K.; Goldstein, A. H.; Guenther, A. B.; Koss, A. R.; Olson, K. F.; de Gouw, J. A.; Baumann, K.; Edgerton, E. S.; Feiner, P. A.; Zhang, L.; Miller, D. O.; Brune, W. H.; Shepson, P. B. Observation of isoprene


DOI: 10.1021/acsearthspacechem.8b00028
*ACS Earth Space Chem.* 2018, 2, 653−672

hydroxynitrates in the southeastern United States and implications for the fate of $NO_x$. *Atmos. Chem. Phys.* **2015**, *15*, 11257−11272.
(31) Lee, B. H.; Mohr, C.; Lopez-Hilfiker, F. D.; Lutz, A.; Hallquist, M.; Lee, L.; Romer, P.; Cohen, R. C.; Iyer, S.; Kurtén, T.; Hu, W.; Day, D. A.; Campuzano-Jost, P.; Jimenez, J.-L.; Xu, L.; Ng, N. L.; Guo, H.; Weber, R. J.; Wild, R. J.; Brown, S. S.; Koss, A.; de Gouw, J.; Olson, K.; Goldstein, A. H.; Seco, R.; Kim, S.; McAvey, K.; Shepson, P. B.; Starn, T.; Baumann, K.; Edgerton, E. S.; Liu, J.; Shilling, J. E.; Miller, D. O.; Brune, W. H.; Schobesberger, S.; D'Ambro, E. L.; Thornton, J. A. Highly functionalized organic nitrates in the southeast United States: Contribution to secondary organic aerosol and reactive nitrogen budgets. *Proc. Natl. Acad. Sci. U. S. A.* **2016**, *113* (6), 1516−1521.
(32) Lopez-Hilfiker, F. D.; Mohr, C.; Ehn, M.; Rubach, F.; Kleist, E.; Wildt, J.; Mentel, T. F.; Lutz, A.; Hallquist, M.; Worsnop, D.; Thornton, J. A. A novel method for online analysis of gas and particle composition: description and evaluation of a Filter Inlet for Gases and AEROsols (FIGAERO). *Atmos. Meas. Tech.* **2014**, *7*, 983−1001.
(33) Lee, B. H.; Lopez-Hilfiker, F. D.; Mohr, C.; Kurtén, T.; Worsnop, D. R.; Thornton, J. A. An Iodide-Adduct High-Resolution Time-of-Flight Chemical-Ionization Mass Spectrometer: Application to Atmospheric Inorganic and Organic Compounds. *Environ. Sci. Technol.* **2014**, *48* (11), 6309−6317.
(34) Paatero, P.; Tapper, U. Positive matrix factorization: a non-negative factor model with optimal utilization of error estimates of data values. *Environmetrics* **1994**, *5*, 111−126.
(35) Zhang, Q.; Jimenez, J.-L.; Canagaratna, M. R.; Ulbrich, I. M.; Ng, N. L.; Worsnop, D. R.; Sun, Y. Understanding atmospheric organic aerosols via factor analysis of aerosol mass spectrometry: a review. *Anal. Bioanal. Chem.* **2011**, *401* (10), 3045−3067.
(36) Huey, L. G.; Hanson, D. R.; Howard, C. J. Reactions of $SF_6$- and I- with atmospheric trace gases. *J. Phys. Chem.* **1995**, *99* (14), 5001−5008.
(37) Heinritzi, M.; Simon, M.; Steiner, G.; Wagner, A. C.; Kürten, A.; Hansel, A.; Curtius, J. Characterization of the mass-dependent transmission efficiency of a CIMS. *Atmos. Meas. Tech.* **2016**, *9*, 1449−1460.
(38) Stark, H.; Yatavelli, R. L. N.; Thompson, S. L.; Kimmel, J. R.; Cubison, M. J.; Chhabra, P. S.; Canagaratna, M. R.; Jayne, J. T.; Worsnop, D. R.; Jimenez, J.-L. Methods to extract molecular and bulk chemical information from series of complex mass spectra with limited mass resolution. *Int. J. Mass Spectrom.* **2015**, *389*, 26−38.
(39) Ulbrich, I. M.; Canagaratna, M. R.; Zhang, Q.; Worsnop, D. R.; Jimenez, J.-L. Interpretation of organic components from Positive Matrix Factorization of aerosol mass spectrometric data. *Atmos. Chem. Phys.* **2009**, *9*, 2891−2918.
(40) Kendrick, E. A mass scale based on $CH_2$ = 14.00000 for high resolution mass spectrometry of organic compounds. *Anal. Chem.* **1963**, *35* (13), 2146−2154.
(41) Kroll, J. H.; Donahue, N. M.; Jimenez, J.-L.; Kessler, S. H.; Canagaratna, M. R.; Wilson, K. R.; Altieri, K. E.; Mazzoleni, L. R.; Wozniak, A. S.; Bluhm, H.; Mysak, E. R.; Smith, J. D.; Kolb, C. E.; Worsnop, D. R. Carbon oxidation state as a metric for describing the chemistry of atmospheric organic aerosol. *Nat. Chem.* **2011**, *3*, 133−139.
(42) Schobesberger, S.; Junninen, H.; Bianchi, F.; Lönn, G.; Ehn, M.; Lehtipalo, K.; Dommen, J.; Ehrhart, S.; Ortega, I. K.; Franchin, A.; Nieminen, T.; Riccobono, F.; Hutterli, M.; Duplissy, J.; Almeida, J.; Amorim, A.; Breitenlechner, M.; Downard, A.; Dunne, E.; Flagan, R. C.; Kajos, M.; Keskinen, H.; Kirkby, J.; Kupc, A.; Kürten, A.; Kurtén, T.; Laaksonen, A.; Mathot, S.; Onnela, A.; Praplan, A. P.; Rondo, L.; Santos, F. D.; Schallhart, S.; Schnitzhofer, R.; Sipilä, M.; Tomé, A.; Tsagkogeorgas, G.; Vehkamäki, H.; Wimmer, D.; Baltensperger, U.; Carslaw, K. S.; Curtius, J.; Hansel, A.; Petäjä, T.; Kulmala, M.; Donahue, N. M.; Worsnop, D. R. Molecular understanding of atmospheric particle formation from sulfuric acid and large oxidized organic molecules. *Proc. Natl. Acad. Sci. U. S. A.* **2013**, *110* (43), 17223−17228.
(43) Kroll, J. H.; Smith, J. D.; Che, D. L.; Kessler, S. H.; Worsnop, D. R.; Wilson, K. R. Measurement of fragmentation and functionalization pathways in the heterogeneous oxidation of oxidized organic aerosol. *Phys. Chem. Chem. Phys.* **2009**, *11*, 8005−8014.
(44) Jokinen, T.; Sipilä, M.; Richters, S.; Kerminen, V. M.; Paasonen, P.; Stratmann, F.; Worsnop, D. R.; Kulmala, M.; Ehn, M.; Herrmann, H.; Berndt, T. Rapid autoxidation forms highly oxidized $RO_2$ radicals in the atmosphere. *Angew. Chem., Int. Ed.* **2014**, *53*, 14596−14600.
(45) Su, L.; Patton, E. G.; Vilà-Guerau de Arellano, J.; Guenther, A. B.; Kaser, L.; Yuan, B.; Xiong, F.; Shepson, P. B.; Zhang, L.; Miller, D. O.; Brune, W. H.; Baumann, K.; Edgerton, E.; Weinheimer, A.; Misztal, P. W.; Park, J.-H.; Goldstein, A. H.; Skog, K. M.; Keutsch, F. N.; Mak, J. E. Understanding isoprene photooxidation using observations and modeling over a subtropical forest in the southeastern US. *Atmos. Chem. Phys.* **2016**, *16*, 7725−7741.
(46) Fry, J. L.; Draper, D. C.; Zarzana, K. J.; Campuzano-Jost, P.; Day, D. A.; Jimenez, J.-L.; Brown, S. S.; Cohen, R. C.; Kaser, L.; Hansel, A.; Cappellin, L.; Karl, T.; Hodzic Roux, A.; Turnipseed, A.; Cantrell, C.; Lefer, B. L.; Grossberg, N. Observations of gas- and aerosol-phase organic nitrates at BEACHON-RoMBAS 2011. *Atmos. Chem. Phys.* **2013**, *13*, 8585−8605.
(47) Kirkby, J.; Duplissy, J.; Sengupta, K.; Frege, C.; Gordon, H.; Williamson, C.; Heinritzi, M.; Simon, M.; Yan, C.; Almeida, J.; Tröstl, J.; Nieminen, T.; Ortega, I. K.; Wagner, R.; Adamov, A.; Amorim, A.; Bernhammer, A.-K.; Bianchi, F.; Breitenlechner, M.; Brilke, S.; Chen, X.; Craven, J.; Dias, A.; Ehrhart, S.; Flagan, R. C.; Franchin, A.; Fuchs, C.; Guida, R.; Hakala, J.; Hoyle, C.; Jokinen, T.; Junninen, H.; Kangasluoma, J.; Kim, J.; Krapf, M.; Kürten, A.; Laaksonen, A.; Lehtipalo, K.; Makhmutov, V.; Mathot, S.; Molteni, U.; Onnela, A.; Peräkylä, O.; Piel, F.; Petäjä, T.; Praplan, A. P.; Pringle, K.; Rap, A.; Richards, N. A. D.; Riipinen, I.; Rissanen, M.; Rondo, L.; Sarnela, N.; Schobesberger, S.; Scott, C. E.; Seinfeld, J. H.; Sipilä, M.; Steiner, G.; Stozhkov, Y.; Stratmann, F.; Tomé, A.; Virtanen, A.; Vogel, A.; Wagner, A. C.; Wagner, P. E.; Weingartner, E.; Wimmer, D.; Winkler, P. M.; Ye, P.; Zhang, X.; Hansel, A.; Dommen, J.; Donahue, N. M.; Worsnop, D. R.; Baltensperger, U.; Kulmala, M.; Carslaw, K. S.; Curtius, J. Ion-induced nucleation of pure biogenic particles. *Nature* **2016**, *533* (7604), 521−526.
(48) Feiner, P. A.; Brune, W. H.; Miller, D. O.; Zhang, L.; Cohen, R. C.; Romer, P. S.; Goldstein, A. H.; Keutsch, F. N.; Skog, K. M.; Wennberg, P. O.; Nguyen, T. B.; Teng, A. P.; de Gouw, J.; Koss, A.; Wild, R. J.; Brown, S. S.; Guenther, A.; Edgerton, E.; Baumann, K.; Fry, J. L. Testing atmospheric oxidation in an Alabama forest. *J. Atmos. Sci.* **2016**, *73*, 4699−4710.
(49) Fry, J. L.; Draper, D. C.; Barsanti, K. C.; Smith, J. N.; Ortega, J.; Winkler, P. M.; Lawler, M. J.; Brown, S. S.; Edwards, P. M.; Cohen, R. C.; Lee, L. Secondary Organic Aerosol Formation and Organic Nitrate Yield from $NO_3$ Oxidation of Biogenic Hydrocarbons. *Environ. Sci. Technol.* **2014**, *48* (20), 11944−11953.
(50) Kurtén, T.; Møller, K. H.; Nguyen, T. B.; Schwantes, R. H.; Misztal, P. K.; Su, L.; Wennberg, P. O.; Fry, J. L.; Kjaergaard, H. G. Alkoxy Radical Bond Scissions Explain the Anomalously Low Secondary Organic Aerosol and Organonitrate Yields From $\alpha$-Pinene + $NO_3$. *J. Phys. Chem. Lett.* **2017**, *8* (13), 2826−2834.
(51) Kulmala, M.; Kontkanen, J.; Junninen, H.; Lehtipalo, K.; Manninen, H. E.; Nieminen, T.; Petäjä, T.; Sipilä, M.; Schobesberger, S.; Rantala, P.; Franchin, A.; Jokinen, T.; Järvinen, E.; Äijälä, M.; Kangasluoma, J.; Hakala, J.; Aalto, P. P.; Paasonen, P.; Mikkilä, J.; Vanhanen, J.; Aalto, J.; Hakola, H.; Makkonen, U.; Ruuskanen, T.; Mauldin, R. L., III; Duplissy, J.; Vehkamäki, H.; Bäck, J.; Kortelainen, A.; Riipinen, I.; Kurtén, T.; Johnston, M. V.; Smith, J. N.; Ehn, M.; Mentel, T. F.; Lehtinen, K. E. J.; Laaksonen, A.; Kerminen, V.-M.; Worsnop, D. R. Direct observations of atmospheric aerosol nucleation. *Science* **2013**, *339* (6122), 943−946.
(52) Wennberg, P. O.; Bates, K. H.; Crounse, J. D.; Dodson, L. G.; McVay, R. C.; Mertens, L. A.; Nguyen, T. B.; Praske, E.; Schwantes, R. H.; Smarte, M. D.; St Clair, J. M.; Teng, A. P.; Zhang, X.; Seinfeld, J. H. Gas-Phase Reactions of Isoprene and Its Major Oxidation Products. *Chem. Rev.* **2018**, *118* (7), 3337−3390.
(53) Krechmer, J. E.; Groessl, M.; Zhang, X.; Junninen, H.; Massoli, P.; Lambe, A. T.; Kimmel, J. R.; Cubison, M. J.; Graf, S.; Lin, Y.-H.;


DOI: 10.1021/acsearthspacechem.8b00028
*ACS Earth Space Chem.* 2018, 2, 653−672

Budisulistiorini, S. H.; Zhang, H.; Surratt, J. D.; Knochenmuss, R.; Jayne, J. T.; Worsnop, D. R.; Jimenez, J.-L.; Canagaratna, M. R. Ion mobility spectrometry−mass spectrometry (IMS−MS) for on- and offline analysis of atmospheric gas and aerosol species. *Atmos. Meas. Tech.* **2016**, *9*, 3245−3262.
(54) Stohl, A.; Eckhardt, S.; Forster, C.; James, P.; Spichtinger, N.; Seibert, P. A replacement for simple back trajectory calculations in the interpretation of atmospheric trace substance measurements. *Atmos. Environ.* **2002**, *36* (29), 4635−4648.
(55) Xu, L.; Middlebrook, A. M.; Liao, J.; de Gouw, J. A.; Guo, H.; Weber, R. J.; Nenes, A.; Lopez-Hilfiker, F. D.; Lee, B. H.; Thornton, J. A.; Brock, C. A.; Neuman, A.; Nowak, J. B.; Pollack, I. B.; Welti, A.; Graus, M.; Warneke, C.; Ng, N. L. Enhanced formation of isoprene-derived organic aerosol in sulfur-rich power plant plumes during Southeast Nexus. *J. Geophys. Res.: Atmos.* **2016**, *121*, 11,137−11,153.
(56) Nouaime, G.; Bertman, S. B.; Seaver, C.; Elyea, D.; Huang, H.; Shepson, P. B.; Starn, T. K.; Riemer, D. D.; Zika, R. G.; Olszyna, K. Sequential oxidation products from tropospheric isoprene chemistry: MACR and MPAN at a NOx-rich forest environment in the southeastern United States. *J. Geophys. Res.* **1998**, *103* (D17), 22463−22471.
(57) Lin, Y.-H.; Zhang, H.; Pye, H. O. T.; Zhang, Z.; Marth, W. J.; Park, S.; Arashiro, M.; Cui, T.; Budisulistiorini, S. H.; Sexton, K. G.; Vizuete, W.; Xie, Y.; Luecken, D. J.; Piletic, I. R.; Edney, E. O.; Bartolotti, L. J.; Gold, A.; Surratt, J. D. Epoxide as a precursor to secondary organic aerosol formation from isoprene photo-oxidation in the presence of nitrogen oxides. *Proc. Natl. Acad. Sci. U. S. A.* **2013**, *110* (17), 6718−6723.
(58) Paulot, F.; Crounse, J. D.; Kjaergaard, H. G.; Kurten, A.; St. Clair, J. M.; Seinfeld, J. H.; Wennberg, P. O. Unexpected epoxide formation in the gas-phase photooxidation of isoprene. *Science* **2009**, *325*, 730−733.
(59) Romer, P. S.; Duffey, K. C.; Wooldridge, P. J.; Allen, H. M.; Ayres, B. R.; Brown, S. S.; Brune, W. H.; Crounse, J. D.; de Gouw, J.; Draper, D. C.; Feiner, P. A.; Fry, J. L.; Goldstein, A. H.; Koss, A.; Misztal, P. K.; Nguyen, T. B.; Olson, K.; Teng, A. P.; Wennberg, P. O.; Wild, R. J.; Zhang, L.; Cohen, R. C. The lifetime of nitrogen oxides in an isoprene-dominated forest. *Atmos. Chem. Phys.* **2016**, *16*, 7623−7637.
(60) Kaiser, J.; Skog, K. M.; Baumann, K.; Bertman, S. B.; Brown, S. S.; Brune, W. H.; Crounse, J. D.; de Gouw, J. A.; Edgerton, E. S.; Feiner, P. A.; Goldstein, A. H.; Koss, A.; Misztal, P. K.; Nguyen, T. B.; Olson, K. F.; St. Clair, J. M.; Teng, A. P.; Toma, S.; Wennberg, P. O.; Wild, R. J.; Zhang, L.; Keutsch, F. N. Speciation of OH reactivity above the canopy of an isoprene-dominated forest. *Atmos. Chem. Phys.* **2016**, *16*, 9349−9359.
(61) Molteni, U.; Bianchi, F.; Klein, F.; El Haddad, I.; Frege, C.; Rossi, M. J.; Dommen, J.; Baltensperger, U. Formation of highly oxygenated organic molecules from aromatic compounds. *Atmos. Chem. Phys.* **2018**, *18*, 1909−1921.
(62) Müller, L.; Reinnig, M.-C.; Naumann, K. H.; Saathoff, H.; Mentel, T. F.; Donahue, N. M.; Hoffmann, T. Formation of 3-methyl-1,2,3-butanetricarboxylic acid via gas phase oxidation of pinonic acid—a mass spectrometric study of SOA aging. *Atmos. Chem. Phys.* **2012**, *12*, 1483−1496.
(63) Canosa-Mas, C. E.; King, M. D.; Scarr, P. J.; Thompson, K. C.; Wayne, R. P. An experimental study of the gas-phase reactions of the $NO_3$ radical with three sesquiterpenes: isolongifolene, alloisolongifolene, and α-neoclovene. *Phys. Chem. Chem. Phys.* **1999**, *1*, 2929−2933.
(64) Pankow, J. F.; Asher, W. E. SIMPOL.1: a simple group contribution method for predicting vapor pressures and enthalpies of vaporization of multifunctional organic compounds. *Atmos. Chem. Phys.* **2008**, *8*, 2773−2796.
(65) Daumit, K. E.; Kessler, S. H.; Kroll, J. H. Average chemical properties and potential formation pathways of highly oxidized organic aerosol. *Faraday Discuss.* **2013**, *165*, 181−202.
(66) Chhabra, P. S.; Lambe, A. T.; Canagaratna, M. R.; Stark, H.; Jayne, J. T.; Onasch, T. B.; Davidovits, P.; Kimmel, J. R.; Worsnop, D. R. Application of high-resolution time-of-flight chemical ionization mass spectrometry measurements to estimate volatility distributions of α-pinene and naphthalene oxidation products. *Atmos. Meas. Tech.* **2015**, *8*, 1−18.
(67) Hu, W.; Palm, B. B.; Day, D. A.; Campuzano-Jost, P.; Krechmer, J. E.; Peng, Z.; de Sá, S. S.; Martin, S. T.; Alexander, M. L.; Baumann, K.; Hacker, L.; Kiendler-Scharr, A.; Koss, A. R.; de Gouw, J. A.; Goldstein, A. H.; Seco, R.; Sjostedt, S. J.; Park, J.-H.; Guenther, A. B.; Kim, S.; Canonaco, F.; Prévôt, A. S. H.; Brune, W. H.; Jimenez, J. L. Volatility and lifetime against OH heterogeneous reaction of ambient isoprene-epoxydiols-derived secondary organic aerosol (IEPOX-SOA). *Atmos. Chem. Phys.* **2016**, *16*, 11563−11580.
(68) Krechmer, J. E.; Day, D. A.; Ziemann, P. J.; Jimenez, J.-L. Direct measurements of gas/particle partitioning and mass accommodation coefficients in environmental chambers. *Environ. Sci. Technol.* **2017**, *51*, 11867−11875.
(69) Mohr, C.; Lopez-Hilfiker, F. D.; Zotter, P.; Prévôt, A. H. S.; Xu, L.; Ng, L. N.; Herndon, S. C.; Williams, L. R.; Franklin, J. P.; Zahniser, M. S.; Worsnop, D. R.; Knighton, B. W.; Aiken, A. C.; Gorkowski, K. J.; Dubey, M. K.; Allan, J. D.; Thornton, J. A. Contribution of Nitrated Phenols to Wood Burning Brown Carbon Light Absorption in Detling, United Kingdom during Winter Time. *Environ. Sci. Technol.* **2013**, *47* (12), 6316−6324.


DOI: 10.1021/acsearthspacechem.8b00028
*ACS Earth Space Chem.* 2018, 2, 653−672